CORRELATION AND EFFECT OF PROCESS PARAMETERS ON THE PROPERTIES OF INCONEL 718 PARTS FABRICATED BY SELECTIVE LASER MELTING USING RESPONSE SURFACE METHOD

by

BHARATH BHUSHAN RAVICHANDER

Presented to the Faculty of the Graduate School of

The University of Texas at Arlington

in partial fulfillment of the requirements

for the degree of

MASTER OF SCIENCE IN MECHANICAL ENGINEERING

THE UNIVERSITY OF TEXAS AT ARLINGTON

May 2020

Acknowledgement

I would like to express my sincerest gratitude to Dr. Narges Shayesteh Moghaddam for being my supervising professor and for providing me with the opportunity to work at the Innovative Additive Manufacturing Lab. This thesis would not have been possible without your guidance, encouragement and ideas. Thank you for sharing your experiences and for the constant motivation throughout the course of my time at the University of Texas at Arlington.

I am also extremely grateful to Dr. Amirhesam Amerinatanzi for his support and guidance throughout the course of this project. Thank you for sharing your expert knowledge on Response Surface Methodology and your dedication to research will always be an excellent example to me.

I sincerely thank my colleagues Mr. Behzad Farhang, Mr. Kiriti Mamidi, Mr. Vignesh Ram Kumar Rajendran and Mr. Himanth Kumar Talla for providing valuable inputs and constructive ideas for the project.

Furthermore, I would also like to thank the members of my committee: Dr. Robert Taylor, Dr. Sunand Santhanagopalan, and Dr. Rassel Raihan for their time, inputs and for providing me with their valuable feedback, Dr. Chen Kan's research group for conducting the roughness analysis, Mr. Kermit Beird, Mr. Rex Winfrey and the staff at the Characterization Center for Materials and Biology lab for allowing me to use their lab equipment as and when necessary.

I would like to heartfully thank my parents who have been a pillar of support and inspiration. Also, my entire family and friends for their constant love, support and encouragement to further pursue my academic interests by supporting me and for making me the person I am today.

Dedicated to

My parents

Abstract

CORRELATION AND EFFECT OF PROCESS PARAMETERS ON THE PROPERTIES OF INCONEL 718 PARTS FABRICATED BY SELECTIVE LASER MELTING USING RESPONSE SURFACE METHOD

Bharath Bhushan Ravichander, M.S

The University of Texas at Arlington, 2020

Supervising Professor: Dr. Narges Shayesteh

Inconel 718 (i.e., IN718) is a nickel-based superalloy that exhibits outstanding tensile and impact-resistant properties, along with good high-temperature corrosion resistance. However, the machinability is poor due to the high stiffness of IN718. Therefore, additive manufacturing provides an effective solution to overcome the work hardening. Selective laser melting (SLM) is the most common powder-bed additive manufacturing technique designed to use a high power-density laser to melt and fuse the metallic powder to fabricate functional parts with high accuracy. However, the accuracy and the functional properties of the fabricated parts are greatly dependent on the process parameters. Thus, depending on the desired properties, the process parameters for a given material need to be optimized for improving the overall reliability of the SLM devices. The processing parameters that control the SLM process comprise of the laser power, scan speed, hatch spacing, and layer thickness. These process parameters are dependent on each other and therefore making the task of optimizing the process parameters an important one.

One of the biggest advantages of optimizing these above-mentioned process parameters is it enables us to control the microstructure as per the requirements. It is important to regulate the microstructure to control the mechanical properties such as tensile strength, yield strength, impact intensity and toughness, as it will directly influence the grain and melt pool distribution in the fabricated parts. As the number of combinations increases, the probability of failure of these additively manufactured parts increases exponentially. As all the process parameters are inter-dependent on each other, finding an optimum value to suit the requirement and render the best build quality both in terms of computer-aided design (CAD)

accuracy and desired metallurgical properties is necessary. Thus, it is essential to determine and establish the optimum combination of values for process parameters.

Design of Experiments (DOE) methodology was used to construct an experiment that evaluated the CAD deviation, composition, hardness and roughness of SLM fabricated IN718 against the three critical processing parameters: laser power, scanning speed and hatch spacing. This work primarily focusses on the effect of various process parameters on the metallurgical properties and mechanical properties of Inconel 718 parts fabricated on an EOS M290 machine.

Table of Contents

List of Tables

List of Figures

Chapter 1. Introduction

1.1. Motivation

The process parameters of additively manufactured parts play a huge role in determining the microstructure and the mechanical properties of the fabricated component. Although additive manufacturing offers great flexibility in design, the CAD geometry may get affected due to the changes in the process parameters. Process parameters also play an important role in determining the type of the grains size and shape, melt pools and composition of different phases which in turn dictates the mechanical properties such as hardness, roughness, tensile and compressive strengths of the fabricated parts. Therefore, the process of optimizing the process parameters helps us in understanding the impact of these process parameters on microstructural and mechanical properties. This understanding of the process parameters shall provide feasibility to dynamically control the build process and thus, can be made more efficient, thereby reducing the post-processing operations.

1.2. Objectives

This work primarily focusses on the optimization of process parameters to control the microstructural properties and mechanical properties of parts fabricated on an EOS M290 machine. Microstructural analysis and compositional analysis are performed on the fabricated parts and they are followed with mechanical analysis like hardness and roughness tests to establish their mechanical properties. Finally, the study is concluded by co-relating the effect of laser power, scan speed and hatch spacing with that of the microstructural and mechanical properties to figure out the best combination of these process parameters for a specific requirement.

1.3.Approach

In the beginning, a detailed literature review was performed on the basic properties of IN718, fabrication of IN718 alloy through SLM technique, effect of process parameters on the microstructural and mechanical properties of IN 718, and the process optimization techniques. Next, after using the Response

Surface Methodology to compile a list of process parameters, the samples of IN718 are fabricated using the SLM technique. After the successful fabrication of these samples, the samples were scanned with a Coordinate Measuring Machine (CMM) to determine the dimensional accuracy of the parts. This was followed by XRD and hardness analysis to find out the composition and hardness values of the IN718 samples.

1.4.Outline

In Chapter 1, the motivation and objectives of the research are presented. This is followed by a comprehensive literature review on IN718 superalloys and Selective Laser Melting (SLM) of IN718 in chapter 2. Chapter 3 covers the fabrication and experimental procedures. Later in Chapter 4, we focus on the results obtained from the dimensional, microstructural, compositional, hardness and roughness analysis and then factorize a relationship of the results obtained above with the process parameters. Finally, chapter 5 discusses the proposed work needed to further complete this research project in the future.

1.5. Contribution

At completion, this research will come up with the following contribution:

1. An understanding of the effect of process parameters on the CAD deviation, compositional properties, and mechanical behavior of SLM fabricated Inconel 718.
2. Establish the co-relation between the geometrical information, microstructure, composition and mechanical properties of SLM fabricated Inconel 718 using Response Surface Methodology (RSM) technique.

1.6. Publications

1. Farhang B, Ravichander BB, Venturi F, Amerinatanzi A, Moghaddam NS. Study on variations of microstructure and metallurgical properties in various heat-affected zones of SLM fabricated Nickel–Titanium alloy. Materials Science and Engineering: A. 2020 Feb 13;774:138919.

2. Ravichander BB, Farhang B, Swails N, Amerinatanzi A, Moghaddam NS. Analysis of the deviation in properties of selective laser melted samples fabricated by varying process parameters. InBehavior and Mechanics of Multifunctional Materials IX 2020 Apr 22 (Vol. 11377, p. 113771A). International Society for Optics and Photonics.
3. Rajendran VR, Mamidi K, Ravichander B, Farhang B, Amerinatanzi A, Moghaddam NS. Determination of residual stress for Inconel 718 samples fabricated through different scanning strategies in selective laser melting. InBehavior and Mechanics of Multifunctional Materials IX 2020 May 21 (Vol. 11377, p. 1137719). International Society for Optics and Photonics.
4. Mamidi K, Talla HK, Ravichander BB, Farhang B, Moghaddam NS, Amerinatanzi A. Study on the influence of post-processing parameters over microstructure and metallurgical properties of NiTi alloy. InBehavior and Mechanics of Multifunctional Materials IX 2020 May 18 (Vol. 11377, p. 113770V). International Society for Optics and Photonics.
5. Srivathsan S, Ravichander BB, Moghaddam NS, Swails N, Amerinatanzi A. Investigation of the strength of different porous lattice structures manufactured using selective laser melting. InBehavior and Mechanics of Multifunctional Materials IX 2020 Apr 22 (Vol. 11377, p. 113771B). International Society for Optics and Photonics.
6. Thakare S, Ravichander BB, Swails N, Moghaddam NS, Amerinatanzi A. The effect of support structure geometry on surface topography of selectively laser melted parts. InBehavior and Mechanics of Multifunctional Materials IX 2020 Apr 22 (Vol. 11377, p. 113771D). International Society for Optics and Photonics.

Chapter 2. Background and Literature Review

2.1. Inconel 718 Superalloys

2.1.1. History of IN718 Superalloys

Inconel 718 (i.e., IN718) is an age-hardenable nickel-based superalloy which was developed in the 1960s by the International Nickel Company [1, 2]. IN718 superalloy is relatively insensitive to strain-age cracking and is found to have excellent weldability properties. This superalloy shows good mechanical and chemical properties even at extreme temperatures such as temperatures near their melting points. The working temperature of this alloy is ranging from -257 ℃ to 704 ℃ [3]. IN718 is also known for its corrosion resistance behavior, high creep resistance behavior and high strength [4]. Thus, IN718 is called a "superalloy" [5]. Due to these properties of IN718, they have applications in the fields such as nuclear power plants, gas turbines, aircraft engines, and combustion chambers [2]. The high presence of Fe and Co makes IN718 economical to use and thus making it one of the most used alloys in the field of oil and gas [6]. IN718 is one of the most commonly used superalloys and accounts for about 35% of all superalloys produced in the 1980s and about 50% of the currently available engines [7].

2.1.2. Phase formation of IN718

IN718 is composed of chromium, molybdenum, aluminum, titanium, cobalt, niobium and nickel with nickel being the biggest contributor [8]. The elements in IN718 are designed to precipitate and form other phases that provide favorable properties depending on the working requirements [9, 10]. The most commonly seen phases in IN718 are γ, γ', γ", δ, MC and laves and their crystal structure and chemical formula are mentioned in table 1.

Table 1: The phases commonly seen in IN718 [8].

Phase	Crystal structure	Chemical formula
γ	Face Centered Cube	Ni
γ′	Face Centered Cube	Ni_3(Al, Ti)
γ″	Body-Centered Tetragonal	Ni_3Nb
δ	Orthorhombic	Ni_3Nb
MC	Cubic	(Nb,Ti)C
Laves	Hexagonal	$(Ni,Fe,Cr)_2(Nb,Mo,Ti)$

The major phase of IN718 is the gamma (γ) phase as it is mainly comprised of Ni and forms austenitic face-centered-cubic (FCC) matrix [11, 12]. IN718 also consists of some secondary phases which are derived mainly from the γ phase and play an important role in determining the microstructure and mechanical properties of IN718. The gamma prime (γ') phase consists of Ni_3(Al, Ti) and is known as the strengthening phase of IN718 and has an FCC crystal structure [13]. γ' phase precipitates homogeneously throughout the matrix and stabilizes against dissolution. Gamma double prime (γ'') phase is another commonly found phase of IN718 and has a body-centered tetragonal crystal structure and contains Ni_3Nb [14]. γ'' and γ’ are the strengthening phases of IN718. γ'' phase found to comparatively higher than that of γ’ and thus it is the prevalent strengthening phase in IN718 [15]. After the γ’ and γ'' phases, the delta phase (δ) can be generally seen in IN718 and contains an orthorhombic crystal structure. δ phase is usually preceded by the γ'' phase and is known to be thermally stable. An increase in the δ phase at the expense of the γ'' phase, leads to lower yield strength and tensile strength values [16, 17]. It must also be noted that the δ phase is found to decrease the ductility of IN718. Thus, average quantities of δ phase at the grain boundaries are helpful as it resists the creep fracture at the grain boundaries. But, large quantities of the δ phase will have a negative effect on the plasticity and strength of IN718 [11, 16, 18].

2.1.3. Conventional Manufacturing of IN718

IN718 is widely manufactured using various conventional manufacturing processes like casting and powder metallurgy. Casting is one of the most commonly used manufacturing techniques. Casting process involves pouring of molten material into a mold cavity that is in the form of the final designed part.

The molten metal is then allowed to cool down and solidify. The mold is later removed and we get the final part [19]. IN718 cast is found to be fundamentally stronger at higher temperatures due to the presence of coarse grains [11]. Cast IN718 is used in aircraft engines, turbines, and nozzles. Wrought IN718 is used in high quantities as the microstructure of wrought IN718 is more homogenous than cast IN718. Wrought metals process refers to those metals that have been shaped with the help of hammers or other tools and opposite to that of casting which uses a mold to create the geometry of the part. Wrought IN718 is also found to have finer grains than cast IN718. Thus, wrought IN718 have better fatigue strength, rupture properties, and tensile strength and have their applications in gas turbines and in aerospace industry parts that require high impact strength [11]. The casted IN718 specimens must be heat treated at high temperatures to increase their homogenization and in turn improve the mechanical properties of the casted parts [20]. The other commonly used method to manufacture IN718 is powder metallurgy. Powder metallurgy has been used to manufacture high-quality turbines for space vehicles made of IN718 with the ability to withstand high amount stresses at high-temperature ranges [21]. IN718 manufactured using powder metallurgy technique is found to have finer grains and uniform mechanical properties and when heat-treated, the yield strength of these IN718 specimens is found to be close to that of wrought IN718. But it must be noted that wrought IN718 has better ductility and stress rupture properties then that of IN718 manufactured using powder metallurgy [22, 23]. Therefore, heat treatment is required for IN718 manufactured using casting and powder metallurgy to obtain the desired properties. This heat treatment leads to oxidation and thus increases the brittleness of the IN718 specimens [24]. Thus, to overcome these difficulties, additive manufacturing techniques like SLS, EBM, and DED offers a viable solution as their processes allow us to tailor the microstructure based on our needs [25].

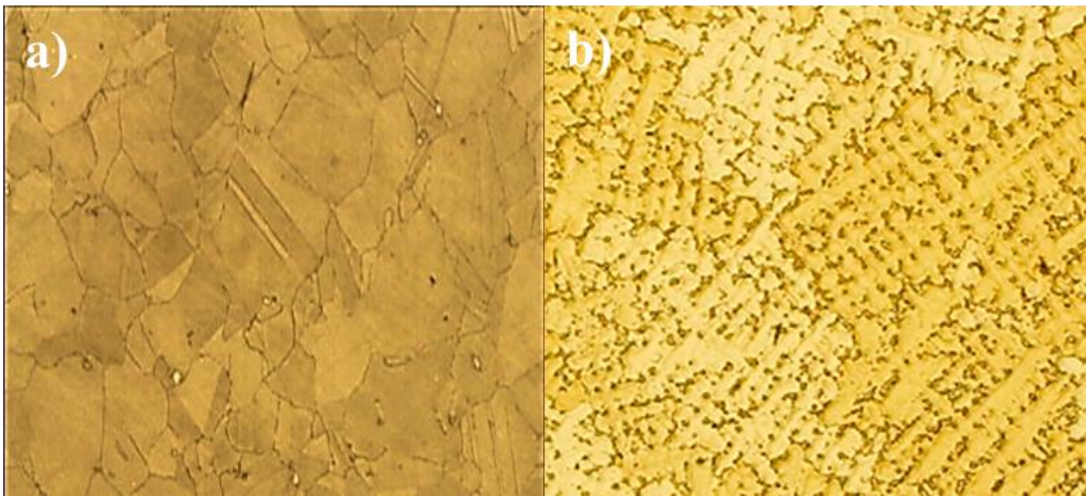

Figure 1: Optical micrographs showing the microstructure of a) Wrought IN718 [26] b) Casted IN718 [27].

2.2 Metal Additive Manufacturing

2.2.1. Introduction and History

Additive Manufacturing or 3d printing is a manufacturing technique that manufactures parts by adding one layer of material on top of another layered material until the part is completed [28, 29]. In recent years, AM technique has been used to fabricate parts with a wide range of materials like metals, polymers, concrete, human tissues, etc [30-33]. AM consists of some techniques like 3d printing, rapid prototyping, direct digital manufacturing [28, 34, 35]. AM techniques add material to obtain the completed part instead of removing the material as done in subtractive manufacturing techniques [36]. In additive manufacturing, the first step is to design and save the required part as a CAD file. The next step is to convert this CAD model into multiple layers and save it as a .stl file. This file is later fed into an AM machine for the parts to be fabricated layer by layer [37] (Figure 2).

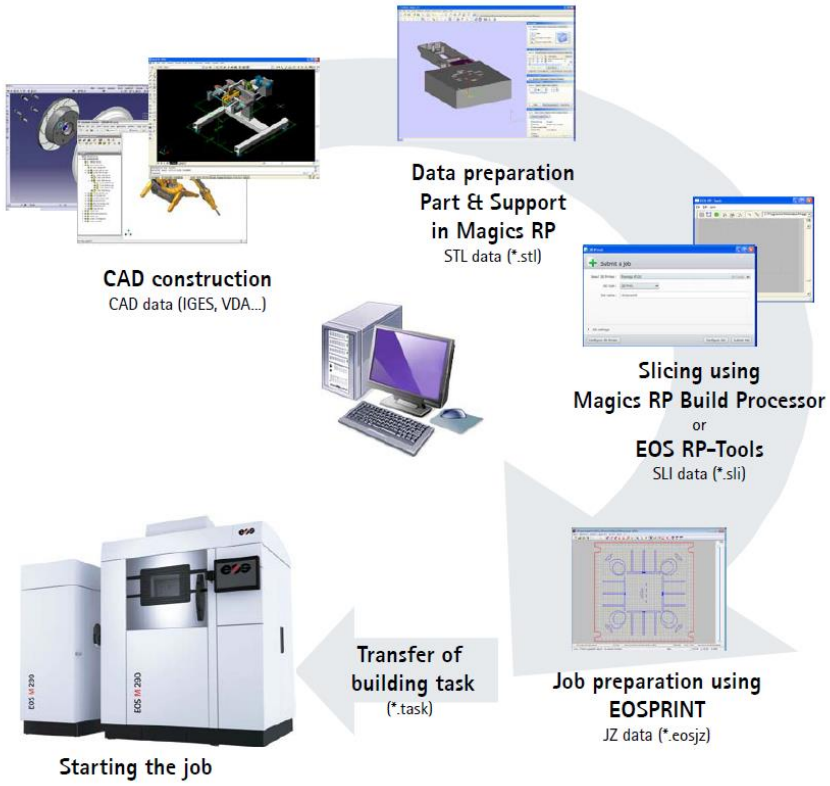

Figure 2: Stages of the additive manufacturing process chain [38].

Additive manufacturing techniques were initially developed around the 1980s. Charles W. Hull of 3D systems corp. developed the first working 3d printer in 1984 [39] and the technique later came to known as Stereolithography. In the mid-1980s, Dr. Carl Deckard and Dr. Joe Beaman started a company named "Betsy" and began their research on a type of technology which used powder to fabricate 3D parts and later patented it under the name "Selective Laser Sintering (SLS)" at the university of Texas [40, 41]. In the late 1990s, Dr. Hans J. Langer started founded EOS and unveiled a direct metal laser sintering (DMLS) machine known as the EOS M250 and later procured the license to manufacture SLS machines from 3D systems [38]. Anderson and Larson developed a new AM technique called electron beam melting (EBM) [42]. In the mid-2000s, Cornell University and the University of Bath together developed the first version of an open-source printer and was based on the fused deposition modeling (FDM) technique [43].

2.2.2. Advantages and Challenges

As AM techniques expand, its technology continues to gain acceptance and makes it a possible way to manufacture parts for many industries. AM techniques enable us to reduce the lead times which in turn leads to a reduction in inventory and thus in costs. Complex parts can be fabricated easily and at a lower cost with the help of AM processes. The other advantage of this manufacturing technique is the ability to manufacture functional parts and thus eliminate the process of assemblies and eradicate excess parts. As these parts are built layer by layer, the amount of material used is comparatively less compared to that of conventional manufacturing. AM techniques allow us to customize parts easily as per the requirement and this is helpful in medical industries and thus helps save lives [39]. While there are many advantages to AM techniques, there are several challenges in this field. One of the biggest challenges of this field is the slow fabricating times and high production costs as the initial setup of some of these techniques are expensive. Post-processing is an integral part of AM and thus leads to changes in the material properties of the fabricated parts. There is a need for skilled labor and machine operators which makes this technique accessible only to a few people. The other challenge of this field is the production rates as only a few parts can be produced at once [44].

2.2.3. Classification of Additive Manufacturing Technology

Additive Manufacturing techniques can be differentiated based on the type of energy source used to fabricate each layer of the part. A wide variety of energy sources like laser-based, electron-based, and ultrasonic based can be used to fabricate samples as per the design requirements. We focus mainly on laser-based additive manufacturing (LBAM) techniques. LBAM processes can be further categorized into three major types:

a) Powder-bed based

b) Flow-based

c) Sheet lamination

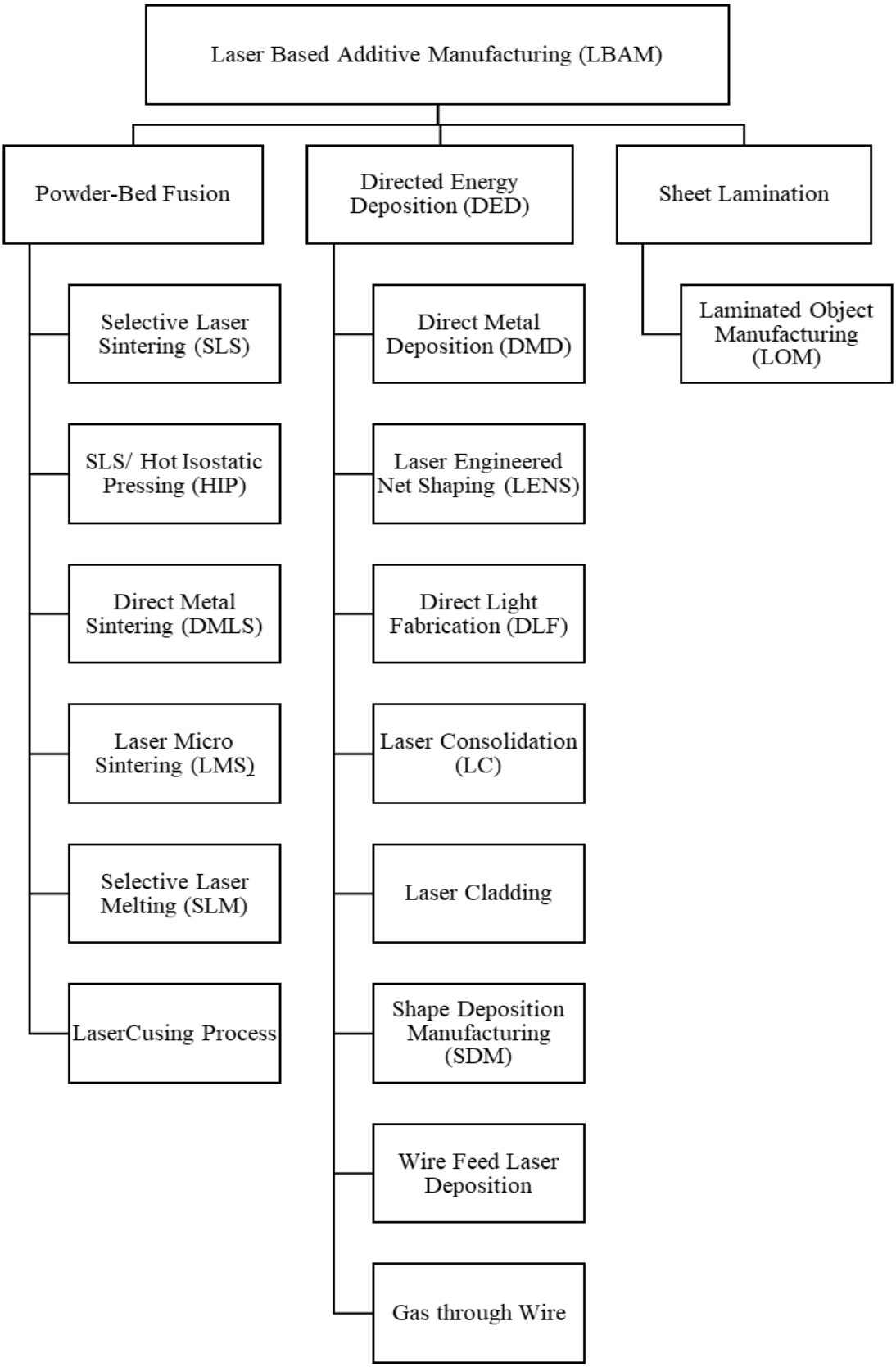

Figure 3: Classification of Laser-Based Additive Manufacturing (LBAM) techniques [45-47].

The above-classified techniques use a wide range of materials like metal powder, metal wires, and metal sheets. Powder bed-based technique can fabricate parts only with the help of powders [48], while wire or powders can be used to fabricate parts using flow-based techniques [49]. Sheet lamination techniques can produce parts only with the help of metal sheets [50]. Powder bed-based techniques are advantageous as the powder particles are small and thus improving the chances of fabricating parts with good dimensional accuracy [51]. On the contrary, flow-based techniques using wire as the material are more eco-friendly as they completely use the material (wire) to fabricate parts and thus reducing wastage [52].

2.2.3.1. Flow-based technique

The flow-based techniques use a nozzle to supply the material to the zone of the laser [49, 53-55]. Flow-based techniques feed the powder to the nozzle with the help of a gas delivery system. This is followed by firing a laser at the center of the nozzle. Finally, a lens is used to focus the laser beam on the workpiece. The movement of the part and the nozzle is controlled using a controller. The workpiece is made to move along the x-y plane, the nozzle moves along the z plane to fabricate the entire part [56]. The flow-based techniques using powder as the material are as follows:

a) Direct metal deposition (DMD)
b) Laser engineered net shaping (LENS)
c) Direct laser fabrication (DLF)
d) Laser consolidation (LC)
e) Laser cladding

2.2.3.2. Powder bed-based technique

The powder bed-based technique uses a device to lay a layer of powder on the printing bed. In this technique, the powder is laid out on the printing bed/substrate. A laser is used to melt the powder and fuse them to form the designed part. The powders around the fabricated part act as a support to the next layer.

The printing bed/substrate goes down by a layer and another layer of powder is laid. As seen in Figure 4, This process continues until the entire part is fabricated [37]. The different types of powder bed-based AM techniques are mentioned below, and further information on each type is provide in Table 2.

a) Selective laser sintering (SLS)

Selective laser sintering (SLS) is a powder bed-based AM technique developed by Dr. Joe Beaman at the university of Texas at Austin in the 1980s [57]. The physical process in SLS can be partial melting or liquid-phase sintering. SLS requires a sacrificial binding material along with the powder particles. A laser is used to melt the binder material and fuse with the powder particles [58]. The melted binder material tends to bind the powder particles around it and they begin to solidify during the cooling down process [59]. The laser does not affect the powder particles at this stage and the parts are around 50% porous and thus are called green parts. Once the fabrication process is complete, the binder material can be removed with the help of heat treatments and this process is known as debinding [60-62].

b) Direct metal laser sintering (DMLS)

Direct metal laser sintering (DMLS) was developed by EOS GmbH and Rapid Product Innovations (RPI) in 1994 [63]. DMLS can be conducted with the help of two different powders or with a single powder have two different grain sizes [62]. This process has the ability to fabricate fully dense parts and this can be achieved by increasing the laser power [64]. One of the biggest advantages of the DMLS technique is that it fabricates parts that are free from internal defects and has the ability to overcome the balling effect.

c) Selective laser melting (SLM)

The SLM technique can be used to fabricate geometrically complex parts with high density (~100%) and thus eradicates the need for post-processing [28, 65-70]. The difference between selective laser sintering (SLS) and the SLM technique is that SLM uses a laser with higher power than that of SLS to fuse the powder completely [71-81]. The major disadvantage of the SLM technique is the resulting residual stress in the samples due to high thermal gradients in the material. This can be overcome by pre-heating the powder material and the maintaining a constant temperature inside the chamber [82].

d) Hot isostatic pressing (HIP)

Hot isostatic pressing (HIP) is a modified version of the SLS technique and was developed at the University of Texas [83]. HIP is a hybrid manufacturing technique that combines both the SLS and HIP in order to fabricate fully dense metal parts at a faster rate [84].

e) Laser micro sintering (LMS)

Laser micro sintering or LMS was announced by Laser Institute Mittelsachsen e.V in 2003. LMS equipment are marketed and sold under the brand name microSINTERING. High resolution and minimum surface roughness can be produced using LMS technique [85]. The other advantage of this technique is that the fabricated parts are free of tension due to the use of q-switched Nd: YAG – laser pulses [86, 87].

f) LaserCusing Process

Laser cusing employs a stochastic exposure strategy. Each layer contains multiple sections called as the island and are fabricated stochastically till the entire layer has been fabricated. The advantage of this technique is the reduction in the inert stress [88-98].

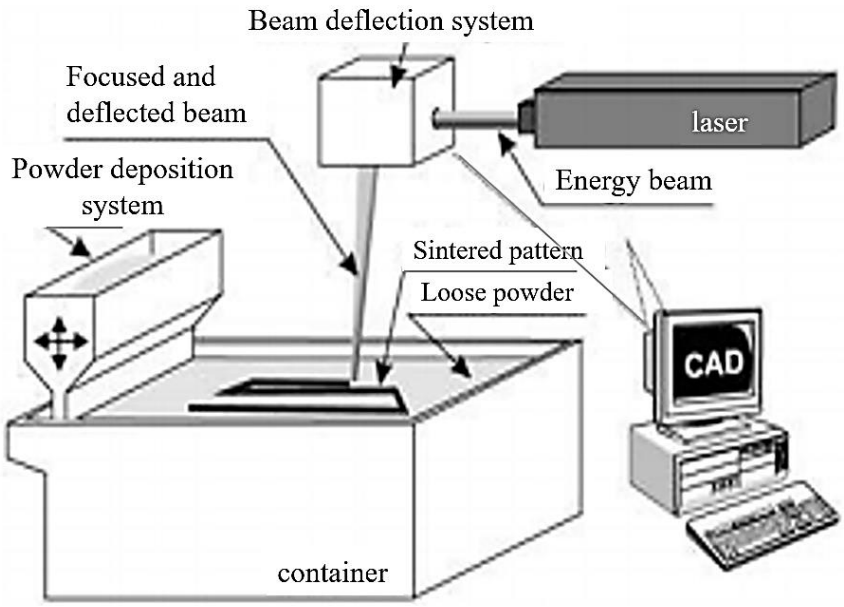

Figure 4: Powder bed-based AM techniques [37].

Table 2: Different types of powder bed-based AM techniques [99].

Powder-bed	Layer Thickness	Common Materials	Resolution	Laser type
SLS	100-300μm [100]	Almost all metallic materials [100]	> 100 μm [101]	CO2 [102], Nd:YAG [103], fiber lasers [104], and disc lasers [105]
SLS/HIP	100-300μm [100]	Inconel 625 superalloy ,Ti-6Al-4V [83, 106]	> 100 μm [101]	CO2 [102], Nd:YAG [103], fiber lasers [104], and disc lasers [105]
DMLS	20-50 μm [63]	Steel alloys, stainless steel, tool steel, aluminum, bronze, cobalt-chrome, (Fe,Ni)–TiC composites and titanium [107]	≈20 μm [108]	CO2 [102], Fiber [104]
LMS	1-10 μm [85]	Steel, silver and copper [85]	<30 μm [85]	Qswitched Nd:YAG in TEM00 mode [85]
SLM	20-100 μm [109]	Stainless steels, aluminum, copper, iron, cobalt chrome, titanium, nickel-based alloy, and a mixture of different types of particles (Fe, Ni, Cu, and Fe3P) [110-112]	≈20 μm [109]	Nd: YAG [113]

In this study, we use the Selective laser melting (SLM) technique to fabricate the IN718 samples.

2.3. Process Parameters and their Influence on the Behavior of SLM IN718

2.3.1. Microstructure in SLM IN718

Studying the microstructure of IN718 specimens fabricated using SLM technique helps us understand the melting and re-melting processes and examine the defects associated with the process. It also enables us to tailor the microstructure as per the requirements [114]. The microstructural analysis of SLM fabricated IN718 samples can be determined with the help of a scanning electron microscope (SEM), optical microscope (OM) and transmission electron microscope (TEM) [115]. In a study conducted by Amato *et al.* [116], it was seen that columnar microstructures are seen parallel to the build direction. Wang *et al.* [114], conducted a similar study and noticed a fine columnar-dendritic microstructure resulted due to high rates of cooling. The presence of columnar grain structures along the build direction in SLM fabricated IN718 has been noted in several studies and is formed as a response to the flow of heat, which is usually seen along the thickness of the samples [116-119]. Brenne *et al.* [120], studied the effect of high laser power

on the microstructure of SLM fabricated IN718 and found columnar grains along the build direction with a high grain aspect ratio compared to the studies which used lower laser power. On the contrary, non-columnar grains were seen in a study conducted by Tucho *et al.* [121]. They concluded that this might have been due to differences in process parameters and boundary conditions compared to other studies [121]. Fine dendritic structures are commonly seen in as built IN718 samples along with phases of laves between the dendritic areas [118, 119, 122].

2.3.2 Mechanical Properties in SLM IN718

Inconel 718 is a precipitate hardened nickel-chromium-molybdenum alloy known for its high strength, corrosion resistance and creep rupture abilities. The mechanical properties of Inconel 718 are primarily necessary as the application of the fabricated part is often dependent on the end-use of the part. Therefore, the use of SLM facilitates us to define and control the mechanical and metallurgical properties of the part. A degradation in properties like tensile and yield strength was observed by Amato *et al.* and Li *et al.* [25, 116]. The difference in the characteristics is attributed to the variation in the governing process parameters [123-133]. The mechanical properties of the cast parts were observed to be inferior to that of the wrought part. Homogenization of microstructure is observed in heat-treated samples [119]. The grain orientations can affect the nature of the parts in terms of ductility. Small and equiaxed grains augment the ductility of the part, whereas the columnar grains shall aid in enhancing the hardness of the alloy specimen [114]. In conjunction with the compositional study of the alloy, hardness and tensile mechanical tests give out a valid interpretation of the idea of choosing SLM for the fabrication of Inconel 718 alloy specimens. The tensile properties of Inconel 718 fabricated using SLM techniques were analogous to that of the wrought specimen [134]. This is due to the high energy imparted to the metal powder by increasing the laser power, which mimics the effects caused by heat treatment of the sample due to prolonged exposure or low scan speeds [135].

2.3.3 Geometrical Accuracy in SLM IN718

Inconel 718 is a superalloy which is widely used in the field of aerospace, biomedical, oil and gas industries. Thus, there is a need for the parts to be fabricated with high dimensional accuracy. Yi *et al.*[136] studied the effect of laser power and scan speed on the geometrical accuracy and noted that as the scan speed decreased and laser power increased, there was an increase in the deviation of the part from the designed CAD model. In a similar study, conducted by Sadowski et al. [137], it was noted that the dimensional accuracy of parts decreased with an increase in laser power. If not chosen properly, the process parameters can cause defects like "balling effect", residual porosity and warpage which affect the dimensional accuracy of the parts [138]. Buchbinder *et al*. [139], improved the accuracy of SLM built parts by preheating the build plate to reduce deformation. Han *et al.*[140], noticed that as the density increased, the geometrical accuracy improved and this was achieved by increasing the scan speed. Di W *et al.* [141] noted that the penetration of the beam width of laser to be the major factor affecting the dimensional accuracy of the fabricated parts.

2.3.4 Hardness Properties in SLM IN718

The process parameters of the SLM technique play a big role in determining the hardness of fabricated IN718 parts [142]. Jia *et al.* [117] conducted a study on the effect of process parameters of SLM on IN718 and noted that as the laser power increases, the hardness of the fabricated parts increases. They also observed that for lower values of laser power, there were low and sporadic hardness values for the samples. Amtao *et al.*[116], determined that as laser power increases, the hardness increases due to an increase in the density and enhancement of the microstructure. The high laser power acts as aging heat treatment to the previously deposited powder layers and thus precipitates the γ' phase which reduces the dislocation and thus increasing the hardness values [116]. In a similar study, Gong *et al.* [143] measured hardness along the build direction and established that the hardness values at the top surface were comparatively higher than that at the bottom surface and concluded that this was due to the presence of laves phases which are brittle in nature. Various hardness analyses, like Vickers and Rockwell test, are

usually conducted to obtain and evaluate the hardness of SLM fabricated components. A hardness of around 500 HV has been reported. Chlebus *et al.* [119] along with Amato *et al.*[116] and Wang *et al.* [114] stated an increase in the hardness values after heat treatment operations.

2.3.5 Roughness Properties in SLM IN718

The surface finish of SLM fabricated IN718 plays a huge role in the application of fabricated part and determines if the part needs post-processing or not. The surface roughness of SLM fabricated IN718 is comparatively high compared to that of traditional manufacturing, and the level of surface roughness depends highly on the employed process parameters [144]. The surface roughness is also known to highly impact the fatigue properties of SLM fabricated parts. In a study conducted by Bean *et al.* [145], it was noted that laser power plays a big role in determining the surface roughness of SLM fabricated IN718 parts. They also established a relationship with surface roughness, density, and porosity. It was seen that surface roughness inversely correlated to density and directly correlated with the porosity of the samples [145]. Yan *et al.* [146] studied the roughness analysis of SLM fabricated parts and established that the high values for R_a was due to the presence of unmelted particles which are formed on the surface due to irregular melting and cooling processes. It was noted that reducing the scan speed and hatch spacing leads to a steady melt pool architecture, resulting in lower values for R_a [147]. In another study conducted by Alrbaey *et al.* [148], it was noted that balling effect increases the surface roughness values and the balling effect can be reduced by melting and re-melting process which in turn enhances the values of R_a by around 80%.

2.3.6 Chemical Composition in SLM IN718

IN718 is chemically composed of the following elements Ni, Cr, Nb, Mo, Ti, Al and Fe. IN718 consists of γ, γ', γ", δ, MC and laves phases. The strengthening phase of IN718 is γ" and this phase can be seen in as-fabricated SLM IN718 [116]. Zhang *et al.* [118] studied the phases of SLM fabricated IN718 and determined that the as-built samples have very few amounts of γ'/γ" precipitates and this is due to the elevated temperature gradient and high solidification rates [149]. It was found that the as-manufactured SLM IN718 had lower strength values compared to that of heat-treated SLM IN718. The heat treatment

leads to the precipitation of γ'/γ" and thus strengthens the matrix material [117, 118, 150, 151]. Niobium segregation can be removed with the help of longer homogenization times or high homogenization temperatures [118, 119]. The texture of as-fabricated IN718 varies with the changes in process parameters. Both <001> building direction [134, 150, 152] textures and isotropic crystallographic orientations were reported [122, 153, 154].

2.4. Optimization of Process Parameters in SLM Processes

The optimization of process parameters such as laser power, scan speed, hatch spacing, layer thickness, laser beam diameter, and position on the substrate in SLM processes is important as the process parameters affect the microstructural property, compositional property, mechanical property, geometrical accuracy and surface finish properties of the fabricated parts. Over the years, very few researchers have tried to optimize these process parameters in order to reduce the variation and establish standard process parameters. As the SLM process is affected by a large number of parameters, a trial and error method would need a very high number of tests and this is not suitable as it would be difficult to determine the correlation between a specific parameter and it's desired value [155]. It must also be noted that this technique is time consuming and expensive. Design of Experiments (DOE) techniques serve as a viable alternative to trial and error methods.

DOE was developed in the 1920s by Sir Ronald Fisher. DOE refers to the practice of planning, designing and analyzing an experiment in order to obtain reasonable conclusions. DOE in manufacturing has two types of variables: Quantitative and Qualitative. Quantitative variable refers to the range of parameters that must be inputted and how to control and measure them during the experiment. Qualitative variable refers to the factors that are discrete during the course of the experiment [156]. Some of the most commonly used DOE types are [157]:

a) Response surface methodology (RSM)
b) Kriging and MP method

c) Taguchian Robust Optimization method

Read *et al.* [158] used the RSM technique to optimize the SLM fabrication of AlSi10Mg alloy. They observed that for a specific energy value, the amount of porosity reduced to close to zero. Maamoun *et al.* [159] conducted a similar study using RSM to optimize the process parameters for AlSi10Mg and Al6061 and noted that for low values of scan speed and high values of laser power, the density of the samples were high. In another study, Zhuang *et al.* [160], studied the effect of the process parameters on the dimensions of the melt pool of Ti6AL4V with the help of the RSM technique and determined that as the laser power increased, the dimensions of the melt pool increased while an increase in the scan speed led to a decrease in the dimensions of the melt pools. Sun *et al.* [161] used the Taguchi method to analyze the effect of the process parameters on the density and established that the thickness of powder plays an important role in determining the density of SLM fabricated Ti6AL4V. Higher laser power and lower scan speeds yielded higher values for hardness for SLM fabricated Ti6AL4V [162].

Chapter 3. Materials and Methods

3.1. Design of Experiments

The purpose of this section is to develop a model to set up a combination of process parameters. The different process parameters involved in the fabrication of IN718 using SLM technique are Laser Power (LP), Scan Speed (SS), Hatch Spacing (HS) and Layer Thickness (LT). To simplify the experiment, LT was kept constant for all the test specimens. The parameters are setup in such a way that it meets the criteria of achieving the best geometrical accuracy, required phase composition and attains the desirable hardness and surface roughness values. Minitab v19 (Minitab Inc., State College, PA, USA) was used in order to establish the Design of Experiments (DOE) matrix. A Central Composite Design (CCD) technique was used in the study as it is the most commonly used Response Surface Methodology (RSM) technique [163]. This technique establishes the standardized efficient parameters and their subsequent relationship by performing the least amount required experiments. Statistically, CCD is an experimental method for the RSM to build a second order design to get an optimized response.

By using the set of defined ranges shown in table 3. for every parameter suggested by CCD approach, a total of 20 different combinations of LP, SS and HS were achieved (Table 4). This was followed by the parts being fabricated with the obtained 20 different process parameters. In the next step, several analysis tests were conducted on the fabricated parts to achieve required results (i.e. geometrical accuracy, required phase composition and attains the desirable hardness and surface roughness values). The observed results were then integrated into a second-order polynomial model and the coefficients of regression were obtained in Minitab v19 (Minitab Inc., State College, PA, USA). Finally, 3D plots and corresponding 2D contours of different parameters were plotted, and then the required parameters were built and marked on each of the 2D contours where the actual CAD geometry, desired phase composition, hardness and surface values is equivalent to that of the desired values [164]. Also, the effect of each parameter and the corresponding required geometrical CAD values, phase composition and the hardness and surface roughness results can be predicted by calculating the value of Δ in the below equation.

$$\Delta = a_1 + a_2 LP - a_3 SS - a_4 HS - a_5 LP^2 + a_6 SS^2 + a_7 HS^2 - a_8 LP \times SS - a_9 LP \times HS + a_{10} SS \times HS \quad \text{Equation 1}$$

Where Δ is the predicted response, a_1-a_{10} are the constants, LP is Laser Power, SS is Scan Speed and HS is the Hatch Spacing.

Table 3: The ranges of effective process parameters.

Factors	**Range and Levels**				
	Low (-1)	**(-α)**	**Central (0)**	**(+α)**	**High (+1)**
Laser Power (W)	237	261	285	309	333
Scan Speed (mm/s)	798	879	960	1041	1122
Hatch Spacing (μm)	92	101	110	119	128

Table 4: The 20 suggested sets of process parameters obtained from RSM technique.

Laser Power (W)	**Scan Speed (mm/s)**	**Hatch Spacing (μm)**
256.5	864.0	99.0
256.5	864.0	121.0
313.5	864.0	121.0
237.1	960.0	110.0
285.0	960.0	110.0
313.5	864.0	99.0
256.5	1056.0	121.0
285.0	960.0	91.5
285.0	960.0	110.0
332.9	960.0	110.0
313.5	1056.0	121.0
285.0	798.5	110.0
285.0	960.0	110.0
285.0	1121.5	110.0
285.0	960.0	110.0
285.0	960.0	110.0
313.5	1056.0	99.0
285.0	960.0	128.5
256.5	1056.0	99.0
285.0	960.0	110.0

3.2. Part Preparation for AM

A total number of 20 rectangular parts (5 mm x 5 mm x 6 mm) were modelled in Solidworks (version 2018-2019, Dassault systems, USA). CAD models was later converted to STL files. Then STL files were loaded into Materialize Magics (Materialize, Leuven, Belgium) for support generation. A 3 mm block support structure having a thickness of 0.3 mm and the gap between each strut was kept at 1 mm. The same support structures were generated for each STL file. Then different process parameter combinations associated with each part were assigned (as described in table 4) using EOS Print 2 (EOS GmbH, Electro Optical Systems, Krailling, Germany). Finally, developed models were then fed into a metal 3D printer for printing using the same software.

3.3. Powder Preparation and Fabrication

The Nickel alloy IN718 powder obtained by gas atomization technique was procured from EOS (EOS GmbH, Electro Optical Systems, Krailling, Germany) whose chemical composition and microstructure are shown in Table 5 and Figure 5, respectively. The average particle size of the powder was around 12 μm.

Table 5: The chemical composition of IN718 super alloy powder.

Element	**Ni**	**Cr**	**Nb**	**Mo**	**Ti**	**Al**	**Fe**
Wt%	50-55	17-21	4.75-5.5	2.8-3.3	0.65-1.15	0.2-0.8	Balance

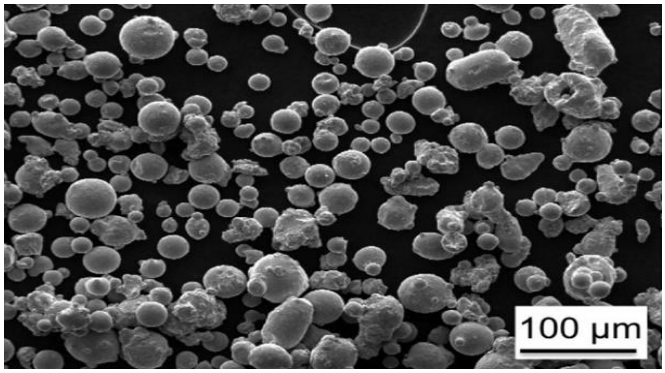

Figure 5: Micrographic image of the EOS IN718 powder.

The powder was sieved before fabrication with mesh size of 90 μm in order to get rid of particulate non homogeneities using the AS 200 Basic Vibratory Sieve Shaker (Retsch, Newtown, Pennsylvania) to maintain the average particle size (Figure 6).

Figure 6: Retsch vibratory sieve shaker.

The parts were printed on a stainless-steel building plate of 250 mm x 250 mm x 25 mm. A DMLS EOS M290 3D printer (EOS GmbH, Electro Optical Systems, Krailling, Germany) equipped with an Ytterbium fiber laser with a power of 400W, shown in Figure 7, was used for fabrication of samples. The solid rectangular samples of 5 x 5 x 6 mm were fabricated with 150 layers of printing. EOS M290 has the ability to fabricate parts with a minimum wall thickness 0.3-0.4 mm and has a minimum density of 8.15 g/cm^3.

Figure 7: EOS M290 metal 3d printer equipped with 400-Watt laser power.

The samples were fabricated using the different values of the process parameters which were obtained by using the principles of Design of Experiments. Response Surface Methodology was adopted to arrive at various combinations of process parameters periodically within a given range.

3.4. Experimental Procedures

3.4.1. Sample Preparation

In this study, the fabricated IN718 samples were removed from the build plate with the help of a band saw. The removed samples were then scanned using a Coordinate Measuring Machine (CMM). Next roughness analysis was performed, and this was followed by hardness analysis. Finally, in order to perform XRD analysis, the samples were cut using a TECHCUT 5™ precision low speed saw demonstrated in Figure 8 (Allied High Tech Products, Inc., Rancho Dominguez, CA). The samples were cut along the XY direction from the top surface and thickness of the cut samples was 2 mm. The thickness of 2 mm was chosen in order to accommodate the part in the XRD sample holder.

Figure 8: Allied TECHCUT 5™ Precision Low Speed Saw.

3.4.2. Coordinate Measuring Machine

A FaroArm® Edge and Laser ScanArm (Faro, Lake Mary, Florida) coordinate measuring machine was used to scan the samples and obtain the data of co-ordinate points (point cloud) of the sample (Figure 9). These co-ordinates were then converted into a CAD model. Finally, the length, width and height of each CAD model were measured using Polyworks Inspector software (Innovmetric, Novi, Michigan).

Figure 9: FaroArm® Edge and Laser ScanArm.

3.4.3. Roughness

Keyence VHX-7000 digital microscope was used to measure surface roughness. The samples were placed on the sample holder and aligned along the edges in order to maintain the consistency of measurements (Figure 10). The controller is used to focus on the sample and three measurements from each side (sides facing the flow of Argon, facing the recoater, facing the observer) were taken. The average values of the roughness for each side has been presented in the result section.

Figure 10: Keyence VHX-7000.

3.4.4. Hardness

A Vickers hardness test was conducted using a LM 300 AT (LECO, St. Joseph, Michigan) micro hardness tester (Figure 11) on each sample. The test was performed by first placing the sample on a sample holder and moving X/Y/Z knob in order to focus the microscopic lens on the surface of sample. A load of 500 g was selected, and the indenter was moved such that it was on top of the sample. The load was applied for a period of 10 seconds. Once the indentation was completed, the indenter was moved again, and the microscopic lens is used to move the crosshairs from one end of the indentation to the other in order to

obtain the values. The hardness test was repeated three times for each side and the average hardness value was reported.

Figure 11: Leco LM 300 AT Micro Hardness Tester.

3.4.5. XRD

A compositional analysis was conducted using a Bruker D8 Advance X-ray diffractometer (XRD) (Bruker Corporation, Madison, WI) (Figure 12) for each fabricated sample. The x-ray source was Cu k-alpha and measurements were made at room temperature with wavelength of 1.5406 Å, step intervals of 0.04° in 2Θ between 30° and 100° and speed of 1 s/step. The XRD results obtained from the Bruker D8 Advance X-ray diffractometer were interpreted using Panalytical X'Pert HighScore Plus (Westborough, MA, USA). The minimum significance of the peaks was kept at 3 for all samples in order to obtain consistent results.

Figure 12: Bruker D8 Advance X-ray diffractometer.

Chapter 4. Results and discussion

4.1. Dimensional analysis

Evaluation of geometrical deviation was carried out on all the 20 fabricated samples with the help of a coordinate measuring machine (CMM). The reason for performing dimensional analysis was to compare the effect of different process parameter combinations on the geometrical accuracy of the fabricated parts and to establish a relationship between process parameters in order to determine an optimized set of parameter range for fabrication. Firstly, it must be noted that higher energy density values lead to an increase in the size of grains and this in turn leads to higher values for height. The energy density also determines the sizes of the melt pool which in sequence changes their dimensions and affects the height of the samples [165]. The values obtained for height were then entered into Minitab and a model was established. In this study, the height of 8 out of the 20 combinations of process parameters exceeded the desired height (max height deviation of 22 μm) while 11 out of the 20 combinations of process parameters resulted in parts whose height were less compared to that of the designed part (max height deviation of 29 μm). The most accurate value for height resulted for the parameter having a laser power of 237 W, scan speed of 960 mm/s and a hatch spacing value of 110 μm which yielded a height of exactly 6 mm. From response surface regression tool in Minitab, the regression equation was found as equation 2.

$$\begin{aligned}\text{Height} = {} & 8.31 - 0.00646\,LP - 0.00178\,SS - 0.0101\,HS + 0.000007\,LP2 + 0.000001\,SS2 \\ & + 0.000041\,HS2 + 0.000001\,LP{\times}SS + 0.000027\,LP{\times}HS - 0.000007\,SS{\times}HS\end{aligned} \quad \text{Equation 2}$$

In a Pareto chart, the effectiveness of the statistical significance of main, square, and interaction of laser processing parameters (LP, HS and SS) on the height of the samples are presented (Figure 11). This chart indicates that scan speed square plays a significant role in determining the height of fabricated IN718 parts. The influence of laser processing parameters is further investigated by the contour and surface plots shown in Figure 14 and Figure 15.

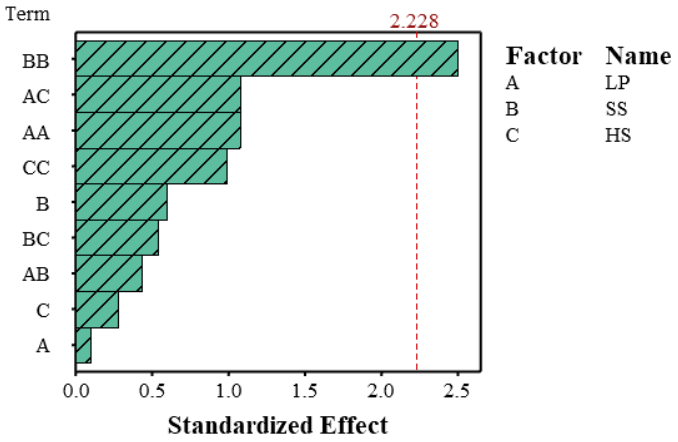

Figure 13: Pareto chart to compare the relative magnitude and the statistical significance of main, square, and interaction of laser processing parameters on the height of fabricated IN718 samples. The reference line on the chart ($\alpha \leq 0.05$) indicates the scan speed square effect on the height is significant.

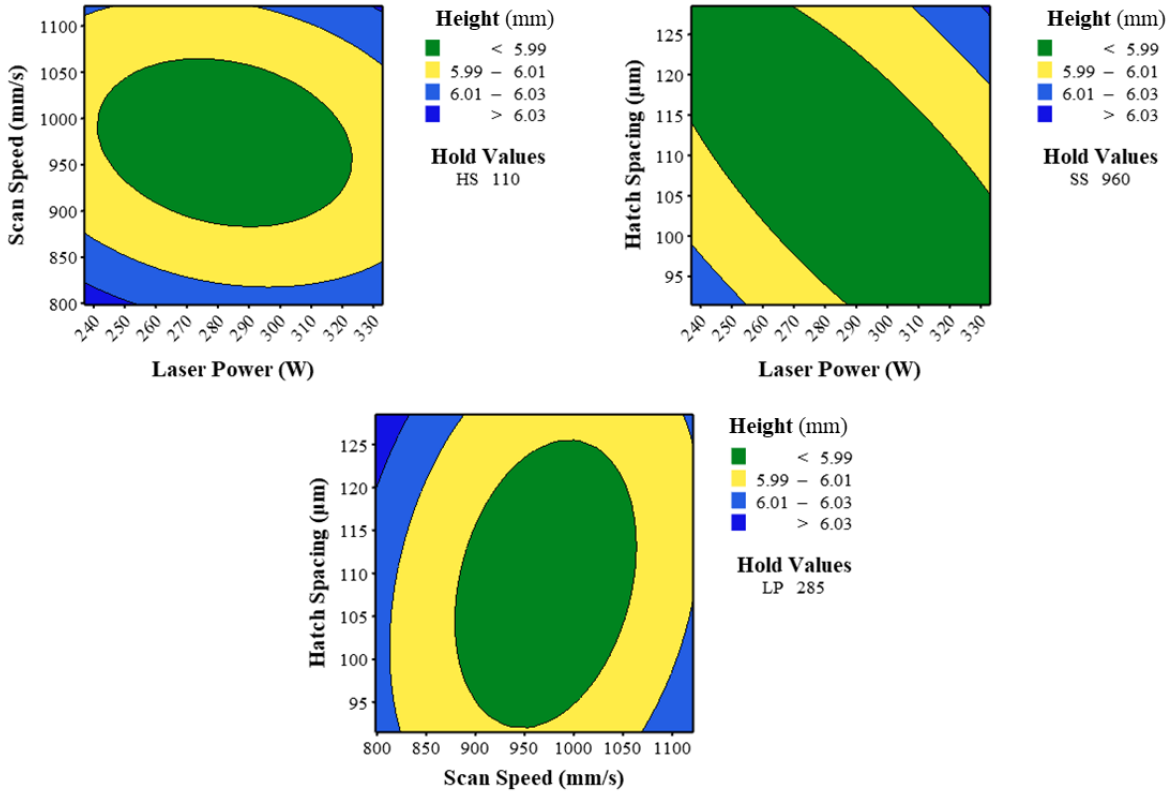

Figure 14: Contour plots showing the effect of different laser processing parameter on the height of fabricated samples. The CAD file was designed with the height of 6 mm. A desired range of 6±0.01 µm is presented as yellow region in the contour plots. The regions in blue and green represent areas of height which are higher and lower than the designed CAD value of 6 mm respectively.

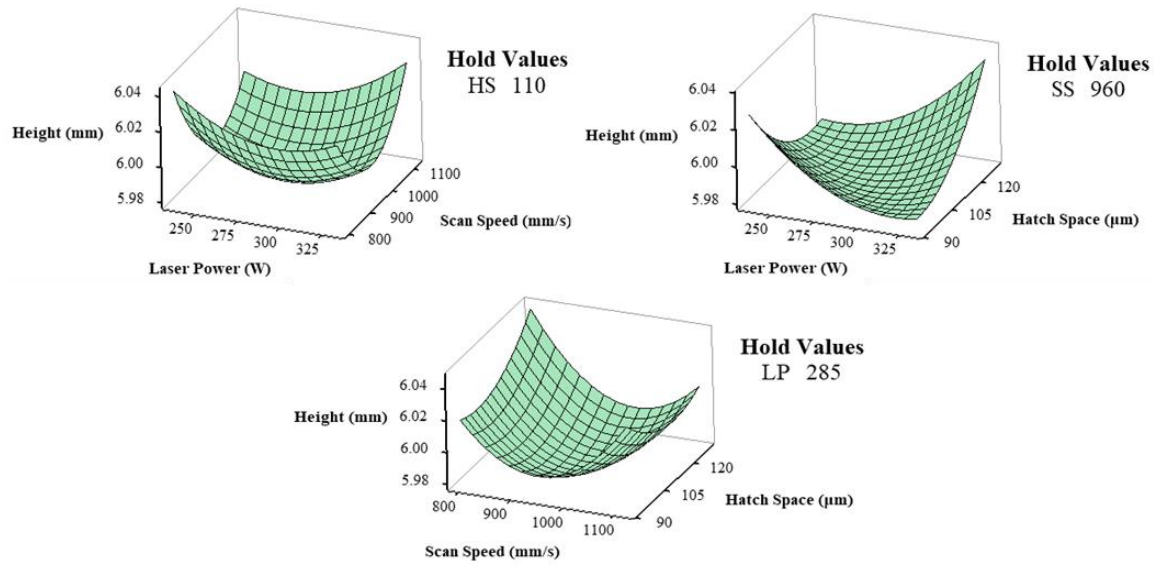

Figure 15: Surface plots showing the effect of different laser processing parameters on the height of fabricated samples.

Secondly, when it came to width, all the 20 samples failed to meet the designed target of 5 mm. The minimum measured width of fabricated samples was 4.981 mm (deviation of 19 µm from the design CAD file). The sample with the closest value to that of the designed value was fabricated with a laser power of 285 W, scan speed of 960 mm/s and a hatch spacing of 110 µm resulted in a part having a width of 5.000 mm. The measured width values were then processed using the response surface regression tool in Minitab in order to establish and analyze the relationship between the width of the fabricated samples and the process parameters. Equation 3 represents the regression of influencing parameters on the width of samples.

$$\text{Width} = 4.679 - 0.00067\,LP + 0.000874\,SS + 0.00045\,HS - 0.000004\,LP^2 - 0.000000\,SS^2 - 0.000001\,HS^2 + 0.000001\,LP{\times}SS + 0.000016\,LP{\times}HS - 0.000004\,SS{\times}HS \quad \text{Equation 3}$$

In a Pareto chart, the effectiveness of the statistical significance of main, square, and interaction of laser processing parameters (LP, HS and SS) on the width of the samples are presented (Figure 14). This chart indicates that scan speed plays a significant role in determining the width of fabricated IN718 parts. Figure 17 and Figure 18 show contour and surface plots of measured width for all fabricated samples. As it is presented, the scan speed plays a major role in establishing the width of an SLM fabricated IN718 part. This trend is different to that observed in the relationship between height and the process parameters.

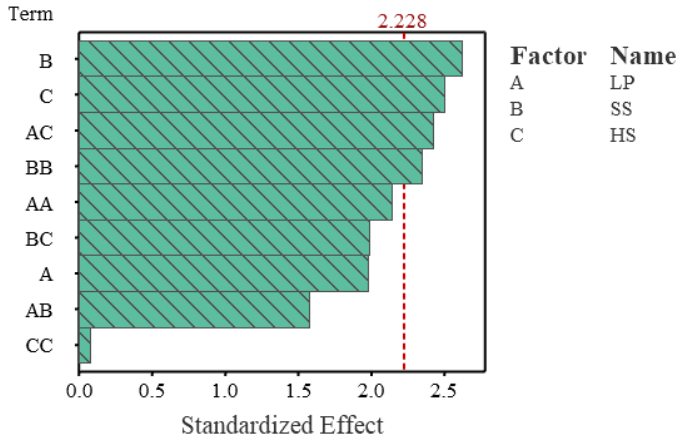

Figure 16: Pareto chart to compare the relative magnitude and the statistical significance of main, square, and interaction of laser processing parameters on the width of fabricated IN718 samples. The reference line on the chart ($\alpha \leq 0.05$) indicates the scan speed effect on the width is significant.

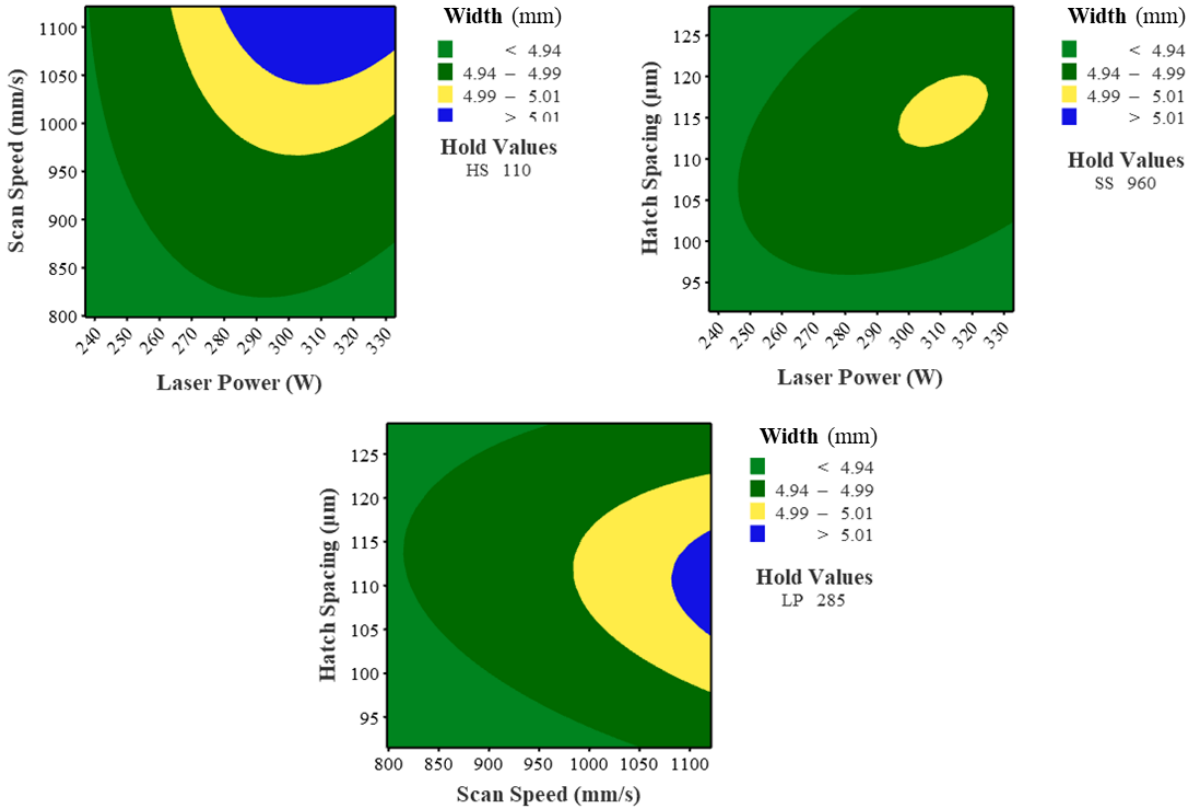

Figure 17: Contour plots showing the effect of different laser processing parameter on the width of fabricated samples. The CAD file was designed with the width of 5 mm. A desired range of 5±0.07 µm is presented as yellow region in the contour plots. The regions in green represent areas of width which are lower than the designed CAD value of 5mm respectively.

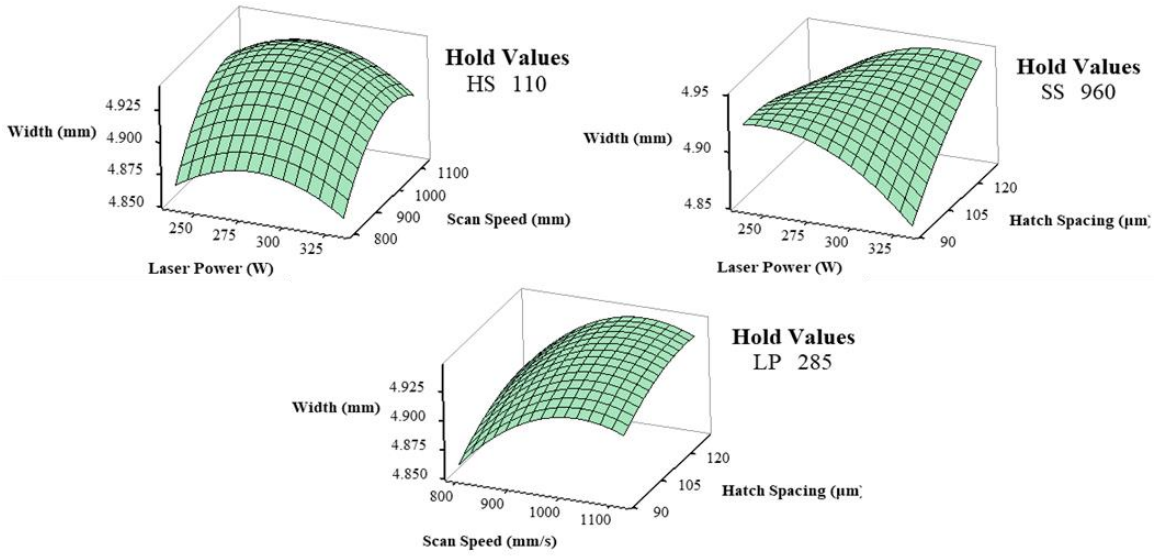

Figure 18: Surface plots showing the effect of different laser processing parameters on the width of fabricated samples.

Finally, the lengths of all the 20 samples were measured and tabulated in Minitab. It was observed that eight of the samples met the design criteria of 5 mm for length. It was also observed that the values for length had a lower range for deviation compared to that of width this is due to growth of grains in the build direction and contraction along the length of the sample [165]. A laser power of 285 W, scan speed of 960 mm/s and a hatch spacing of 110 µm resulted in a sample with a length of 5.000 mm. Equation 4 represents the regression of influencing parameters on the length of samples.

$$\text{Length} = 4.655 - 0.00089\,LP + 0.000753\,SS + 0.00167\,HS - 0.000003\,LP^2 - 0.000000\,SS^2 - 0.000014\,HS^2 + 0.000001\,LP{\times}SS + 0.000013\,LP{\times}HS - 0.000002\,SS{\times}HS \quad \text{Equation 4}$$

In a Pareto chart, the effectiveness of the statistical significance of main, square, and interaction of laser processing parameters (LP, HS and SS) on the length of the samples are presented (Figure 17). This chart indicates that hatch spacing square plays a significant role in determining the length of fabricated IN718parts.

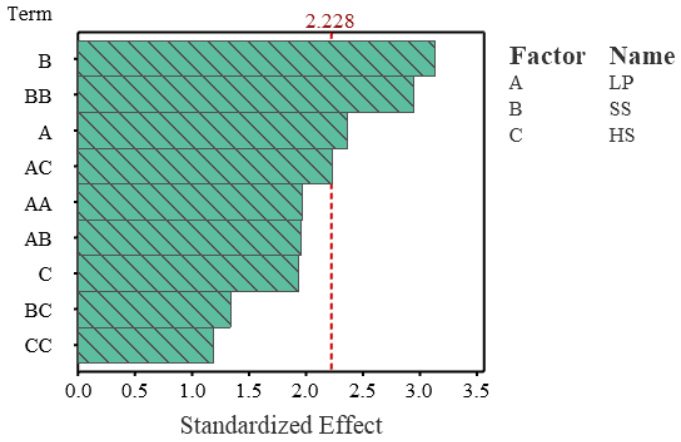

Figure 19: Pareto chart for a reduced model to compare the relative magnitude and the statistical significance of square, and interaction of laser processing parameters on the length of fabricated IN718 samples. The reference line on the chart ($\alpha \leq 0.05$) indicates the hatch space square effect on the length is significant.

From Figure 20 and Figure 21, we can see that hatch spacing affects the length of an as-built part significantly as determined by the response surface regression tool in Minitab.

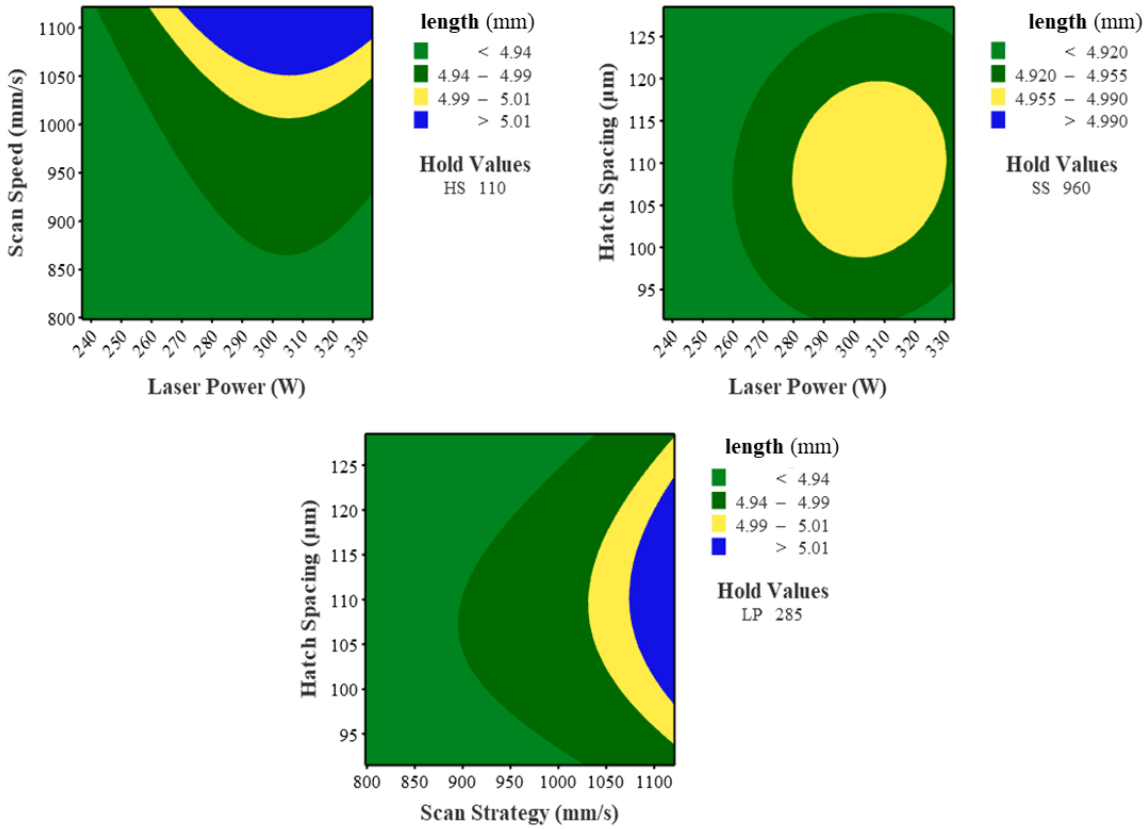

Figure 20: Contour plots showing the effect of different laser processing parameter on the length of fabricated samples. The CAD file was designed with the length of 5 mm. A desired range of 5±0.12 µm is presented as yellow region in the contour plots. The regions in green represent areas of length which are lower than the designed CAD value of 5 mm respectively.

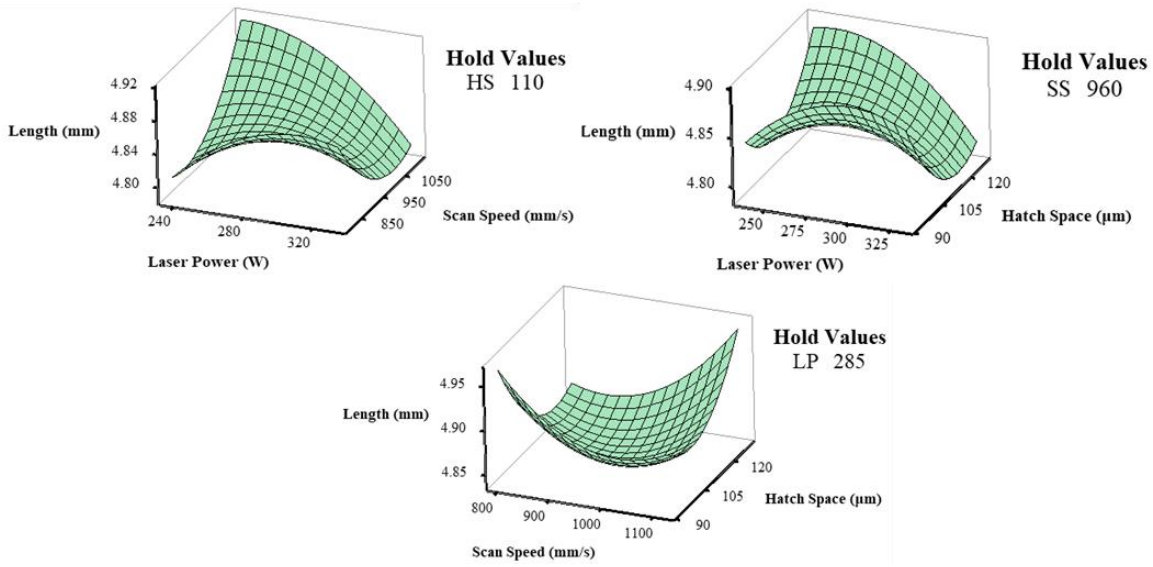

Figure 21: Surface plots showing the effect of different laser processing parameters on the length of fabricated samples.

The mean of measured values for length, width and height along with their corresponding values of different laser process parameters are mentioned in Table 6. As discussed earlier, from the table below it can be deduced that the range of deviation for length is higher than that of width and height. This is due to the contraction as lower energy density leads to faster cooling. Similarly, higher scan speed values have shown increased deviation in length as the laser travels faster thereby imparting significantly lesser energy at the heat zone [165]. Now the deviation in height, can be attributed to the square of scan speed as the scan speed directly influences the energy density. High values for energy density can lead to re-melting of previously solidified layers, thereby intensifying the epitaxial grain growth. Now higher scan speed values do not impart the necessary thermal energy for proper adhesion by re-melting. This shall lead to defects such as porosities and balling effect. The deviation in width can also be related to the main factor scan speed, similar to the above discussed effect of square scan speed on height.

Table 6: Average measured values of length, width and height for all samples compared to the designed CAD values of 5 mm, 5 mm and 6 mm for length, width and height, respectively.

Laser Power (W)	Scan Speed (mm/s)	Hatch Spacing (µm)	Length (mm)	Width (mm)	Height (mm)
256.5	864.0	99.0	5.000	5.001	5.997
256.5	864.0	121.0	4.996	4.997	6.011
313.5	864.0	121.0	4.990	4.997	6.018
237.1	960.0	110.0	4.989	4.987	6.000
285.0	960.0	110.0	5.000	5.000	5.972
313.5	864.0	99.0	4.969	4.965	6.005
256.5	1056.0	121.0	5.000	5.000	5.971
285.0	960.0	91.5	4.987	4.988	5.985
285.0	960.0	110.0	5.000	5.000	5.972
332.9	960.0	110.0	4.990	4.989	5.986
313.5	1056.0	121.0	4.999	4.997	6.011
285.0	798.5	110.0	4.980	4.981	6.007
285.0	960.0	110.0	5.000	5.000	6.021
285.0	1121.5	110.0	4.992	4.993	6.018
285.0	960.0	110.0	5.000	5.000	5.972
285.0	960.0	110.0	5.000	5.000	5.972
313.5	1056.0	99.0	4.994	4.996	5.993
285.0	960.0	128.5	4.994	5.000	5.999
256.5	1056.0	99.0	5.002	5.003	6.022
285.0	960.0	110.0	5.000	5.000	5.972

4.2. Compositional analysis

The compositional analysis was carried out using an X-ray Diffractometer. The resultant XRD graph of all 20 samples are presented in figure 20. As it is shown, the different phases of IN718 included γ, γ', γ" and δ were observed in all 20 fabricated samples.

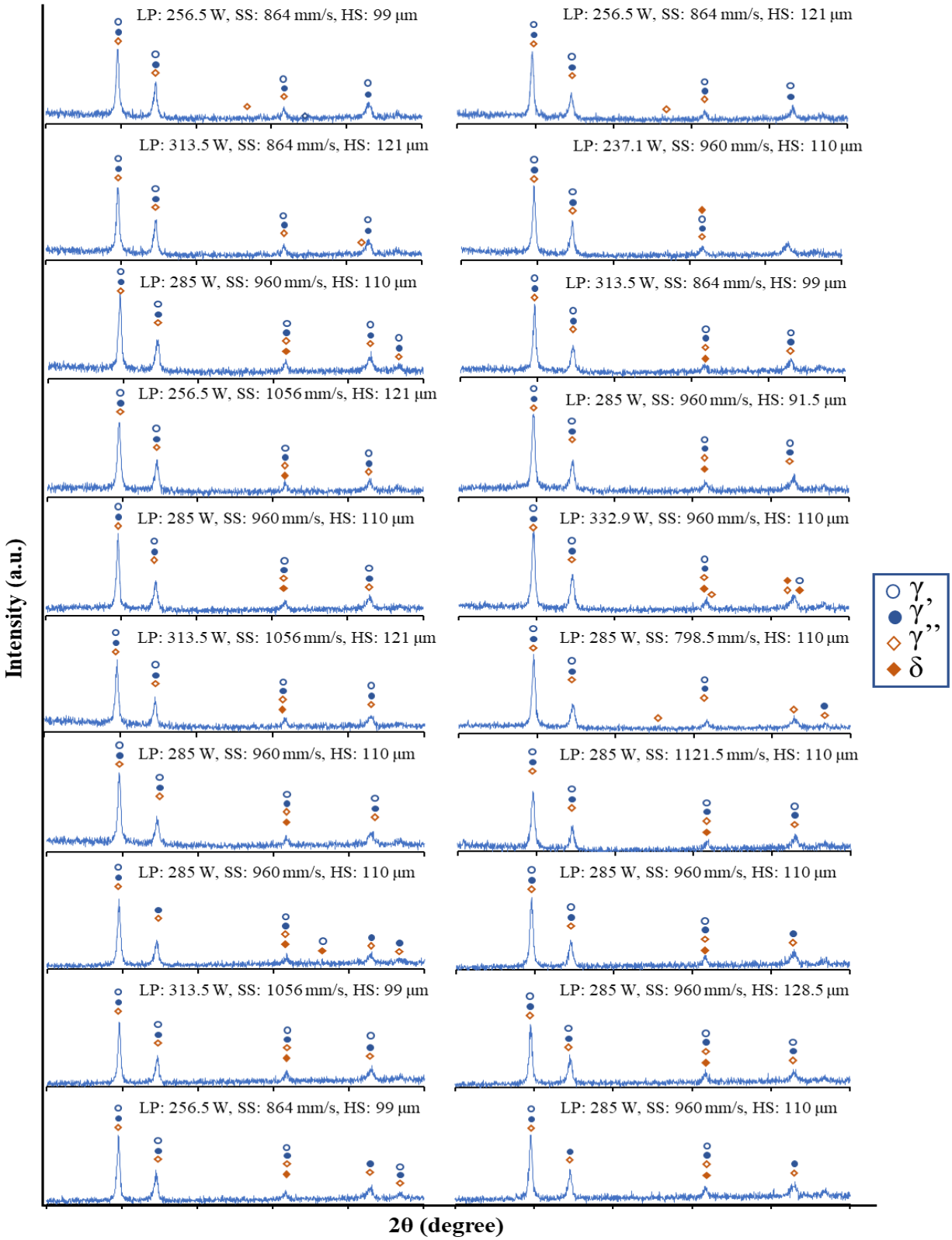

Figure 22: XRD graphs showing the different phases in the IN718 parts fabricated by different laser process parameters.

As it was expected γ phase found to be the major phase in all of the fabricated samples (60-75%) and the rest comprised mostly of γ' and γ" phases (the strengthening phases of IN718). δ phase (the thermally stability phase of IN718) was also presented in traces and had composition similar to that of γ" phase [8]. The γ' phase is one of the primary strengthening phases of IN718 composed of Ni_3 (Al, Ti) and thus its plays an important in mechanical properties of the fabricated sample [8]. A high value of 18.190% for γ' phase was found in a sample which had laser power of 285 W, hatch space of 110 μm and the highest scan speed of 1121.5 mm/s. Equation 5 represents the regression of influencing parameters on the percentage of γ' present in the samples.

$$\gamma' = 193.6 + 0.306\,LP - 0.1669\,SS - 2.425\,HS - 0.000094\,LP^2 + 0.000051\,SS^2 + 0.00641\,HS^2 - 0.000235\,LP{\times}SS - 0.00025\,LP{\times}HS + 0.001097\,SS{\times}HS \quad \text{Equation 5}$$

In a Pareto chart, the effectiveness of the statistical significance of main, square, and interaction of laser processing parameters (LP, HS and SS) on the percentage of γ' present in the samples are presented (Figure 21). This chart indicates that the interaction between scan speed and hatch spacing plays a significant role in determining the percentage of γ' in the fabricated IN718 parts. The chemical and structural compatibility of γ and γ' is high. So, in order to homogeneously disperse γ' into the alloying matrix critical energy density value should be attained [8]. The critical energy density is a factor of scan speed and hatch spacing.

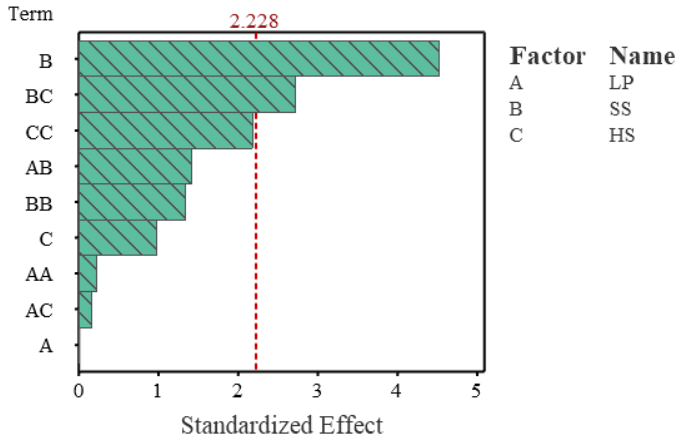

Figure 23: Pareto chart for a reduced model to compare the relative magnitude and the statistical significance of square, and interaction of laser processing parameters on the γ' of fabricated IN718 samples. The reference line on the chart (α ≤0.05) indicates the hatch space square effect on the γ'is significant.

From the contour plots in Figure 24 and the response surface regression tool, it is evident that the combination of scan speed and hatch spacing play an important role in the development of γ' phases.

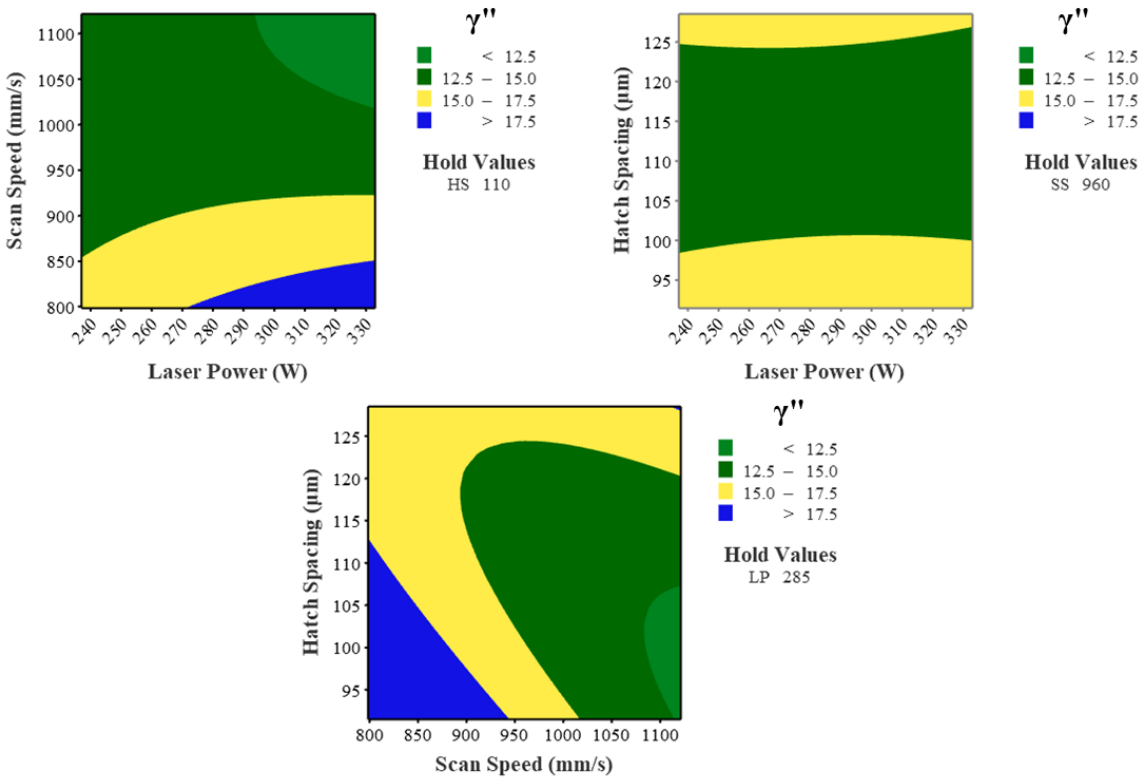

Figure 24: Contour plots showing the effect of different laser processing parameter on the percentage of γ' phase of different samples, the desired ranges for the γ' phase are presented in yellow areas (higher value of γ' phase). The regions in green represent areas of γ' which are lower than the desired value respectively.

4.3. Hardness analysis

Vickers Hardness values were measured on the side facing the recoater (the side facing the pool of fresh powder) for all the 20 samples and the corresponding contour plots are represented in Figure 24. From the response surface regression model, it is seen that laser power and scan speed play a major role in determining the hardness of the sample when it comes to the recoater side. A mid-range value of 256.5 W laser power and a low hatch spacing value of 99 µm and low scan speed value of 864 mm/s resulted in the highest Vickers hardness value of 505.442 HV. This is due to the fact that the employment of high energy

density (78.8 J/mm^2) results in the fully re-melting of the previously melted powder which in turn increases the hardness values [115]. The minimum hardness value of 296.1 HV was noticed as the laser power was increased to its highest value of 332.9 W, while the scan speed and hatch spacing were kept at an optimum value of 960 mm/s and 110 μm. Equation 6 represents the regression of influencing parameters on the hardness of the fabricated samples.

$$\text{Hardness (Recoater side)} = 3730 + 4.9\,LP - 5.43\,SS - 24.3\,HS - 0.0116\,LP^2 + 0.00320\,SS^2 + 0.058\,HS^2 - 0.00306\,LP*SS + 0.0390\,LP*HS \quad \text{Equation 6}$$

In a Pareto chart, the effectiveness of the statistical significance of main, square, and interaction of laser processing parameters (LP, HS and SS) on the hardness of the samples are presented (Figure 23). This chart indicates that the scan speed square plays a significant role in determining the hardness of the fabricated IN718 parts.

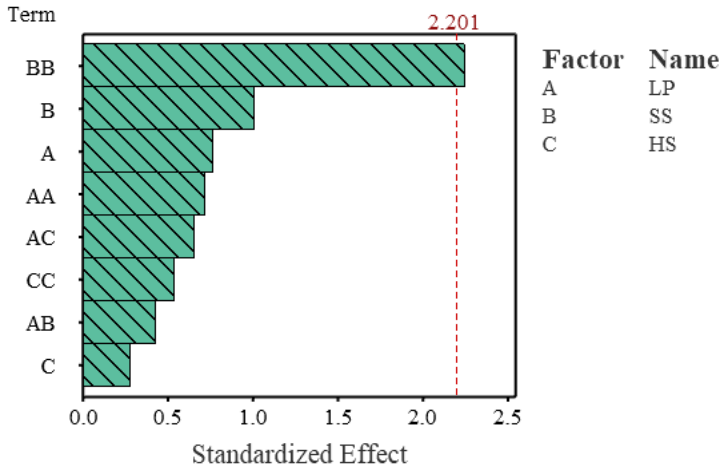

Figure 25: Pareto chart for a reduced model to compare the relative magnitude and the statistical significance of square, and interaction of laser processing parameters on the width of fabricated IN718 samples. The reference line on the chart ($\alpha \leq 0.05$) indicates the hatch space square effect on the hardness is significant.

From the contour plots in Figure 24 and the response surface regression tool, it is evident that the scan speed affects the hardness of the IN718 parts.

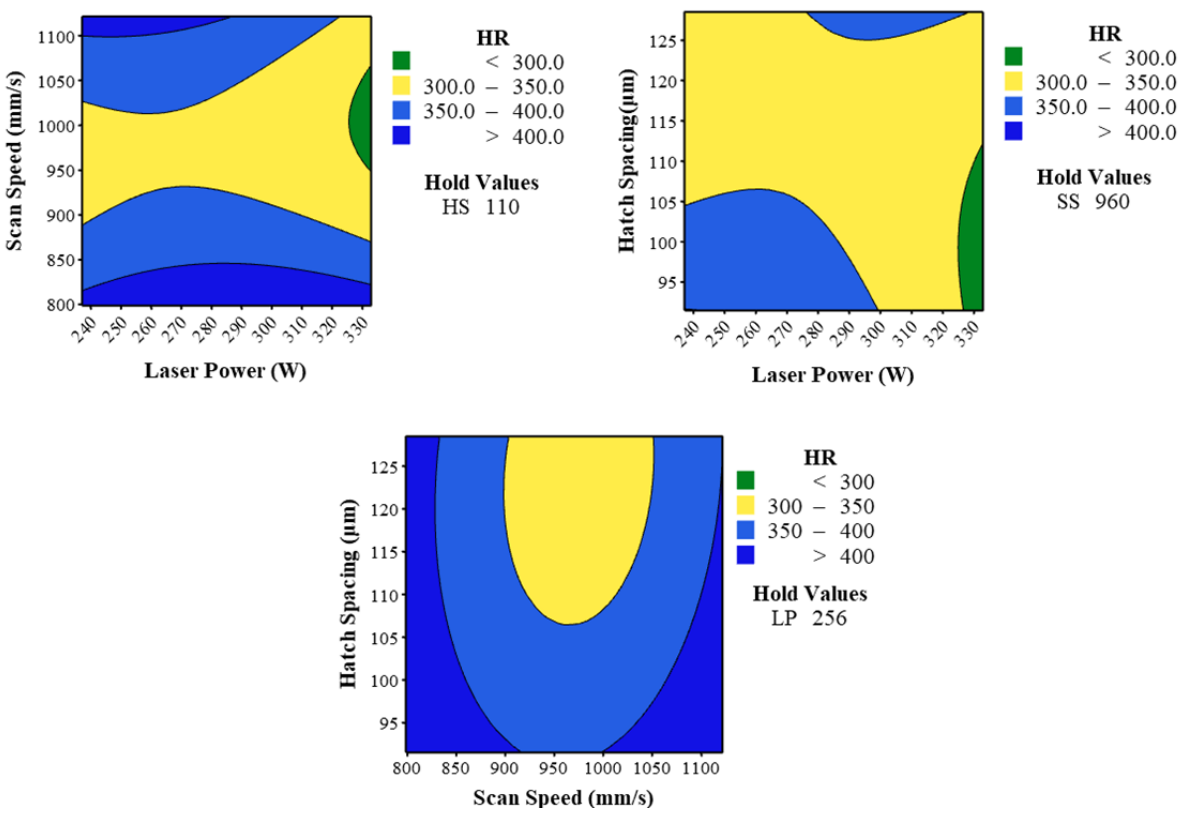

Figure 24: Contour plots showing the effect of different laser processing parameter on the hardness of different samples facing the recoater (the side facing the pool of fresh powder), the desired ranges for the hardness are presented in yellow areas. The regions in blue and green represent areas of hardness which are higher and lower than the desired value respectively.

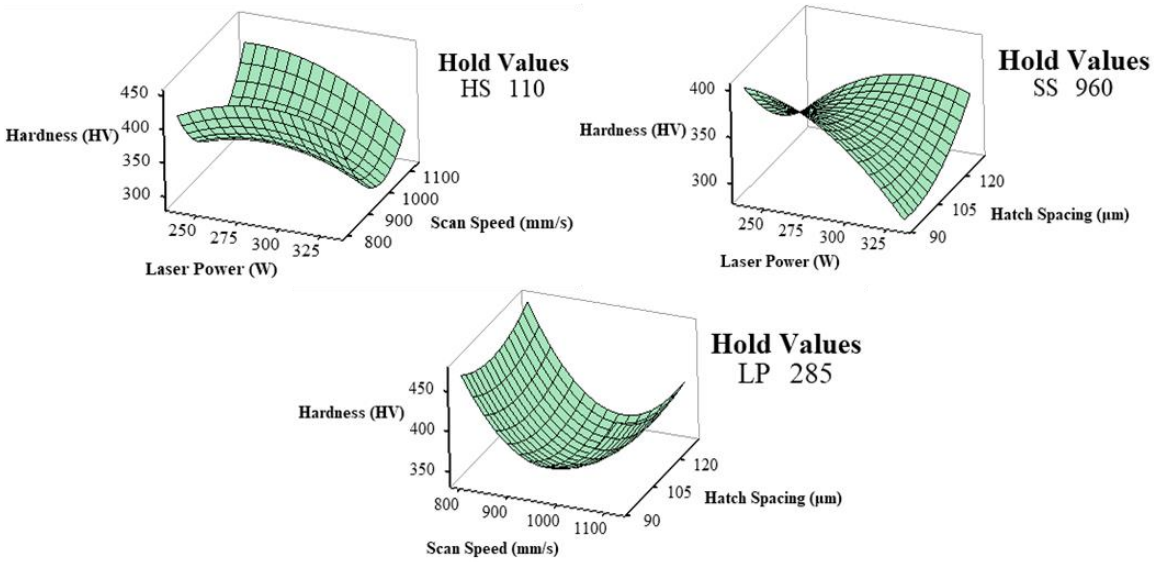

Figure 26: Surface plots showing the effect of different laser processing parameters on the hardness of different samples facing the recoater (the side facing the pool of fresh powder)

The Vickers Hardness tests were conducted on the other sides and the top surface of the samples in order to compare the hardness values on different surfaces and are mentioned in Table 7. Higher values for hardness were observed for the side facing the recoater (the side facing the pool of fresh powder) and the lower hardness values were noted for the top surface of the samples. From the table, it can be inferred that as the laser power increases, the hardness values increase. There are some variations in the relationship between hardness values and laser power, this can be due to the distribution of microstructure on the fabricated parts.

Table 7: Average values of hardness on the sides facing the flow of Argon, facing the recoater, facing the observer and average hardness value of the top surface of all samples

Laser Power (W)	Scan Speed (mm/s)	Hatch Spacing (µm)	Hardness (Argon side)	Hardness (Recoater side)	Hardness (Observer side)	Hardness (Top surface)
256.5	864.0	99.0	370.637	303.444	335.884	272.468
256.5	864.0	121.0	399.567	362.460	357.253	264.722
313.5	864.0	121.0	311.939	406.726	311.745	273.813
237.1	960.0	110.0	471.427	315.604	349.755	260.7017
285.0	960.0	110.0	399.905	321.698	372.848	271.733
313.5	864.0	99.0	398.842	340.209	325.244	308.584
256.5	1056.0	121.0	402.093	395.528	472.897	261.5784
285.0	960.0	91.5	360.151	374.154	383.387	289.544
285.0	960.0	110.0	399.905	321.698	372.848	271.733
332.9	960.0	110.0	374.262	296.136	294.624	270.404
313.5	1056.0	121.0	437.908	343.469	355.872	270.27
285.0	798.5	110.0	341.733	463.262	375.544	285.600
285.0	960.0	110.0	320.029	351.774	305.151	271.733
285.0	1121.5	110.0	321.376	368.830	348.320	265.804
285.0	960.0	110.0	320.029	351.774	305.151	271.733
285.0	960.0	110.0	320.029	351.774	305.151	271.733
313.5	1056.0	99.0	395.409	350.991	373.880	270.39
285.0	960.0	128.5	333.331	331.018	370.368	260.28
256.5	1056.0	99.0	461.763	505.442	327.598	272.468
285.0	960.0	110.0	320.029	351.774	305.151	271.733

4.4. Roughness Analysis

Surface roughness of the fabricated samples were performed using a Keyence microscope and the surface roughness values were tabulated. From Minitab, it was determined that the combination of scan speed and hatch spacing play an important role in the influencing the surface roughness of SLM fabricated IN718. A low value of 2.905 μm for surface roughness as seen in Figure 30 was noted when the scan speed was kept at a low value of 798.5 mm/s while the laser power and hatch spacing were maintained at an optimum value of 285 W and 110 μm respectively. With the help of the regression analysis tool available on Minitab, it was deduced that surface roughness was observed to increase with an increase in scan speed and hatch spacing which might be due to balling effect and unmelted powder at the edges of the samples and this can be seen in Figure 30. The highest value for Sa was observed for the sample when the laser power was 313.5 W, scan speed of 1056 mm/s and a hatch spacing of 121 μm. Equation 7 represents the regression of influencing parameters on the roughness of the fabricated samples.

$$\text{Sa Recoater} = 6492 - 13.81\,LP - 5.66\,SS - 37.1\,HS + 0.00200\,LP^2 + 0.0182\,HS^2 + 0.01006\,LP*SS + 0.0335\,LP*HS + 0.0264\,SS*HS \quad \text{Equation 7}$$

In a Pareto chart, the effectiveness of the statistical significance of main, square, and interaction of laser processing parameters (LP, HS and SS) on the hardness of the samples are presented (figure 25). This chart indicates that the interaction between scan speed and hatch spacing plays a significant role in determining the roughness of the fabricated IN718 parts. It can be observed from the standardized effect chart that various combinations of process parameters directly impact overall roughness of the part. Therefore, it can be inferred that the roughness values are impacted by all the process parameters in varying degrees.

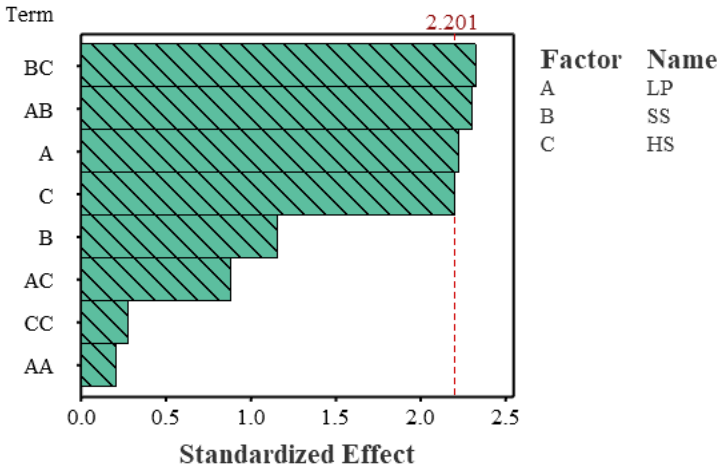

Figure 27: Pareto chart for a reduced model to compare the relative magnitude and the statistical significance of square, and interaction of laser processing parameters on the width of fabricated IN718 samples. The reference line on the chart ($\alpha \leq 0.05$) indicates the hatch space square effect on the roughness is significant.

Contour plots and surface plots of roughness analysis for the side facing the recoater (the side facing the pool of fresh powder) are shown in Figure 20 and Figure 21, respectively.

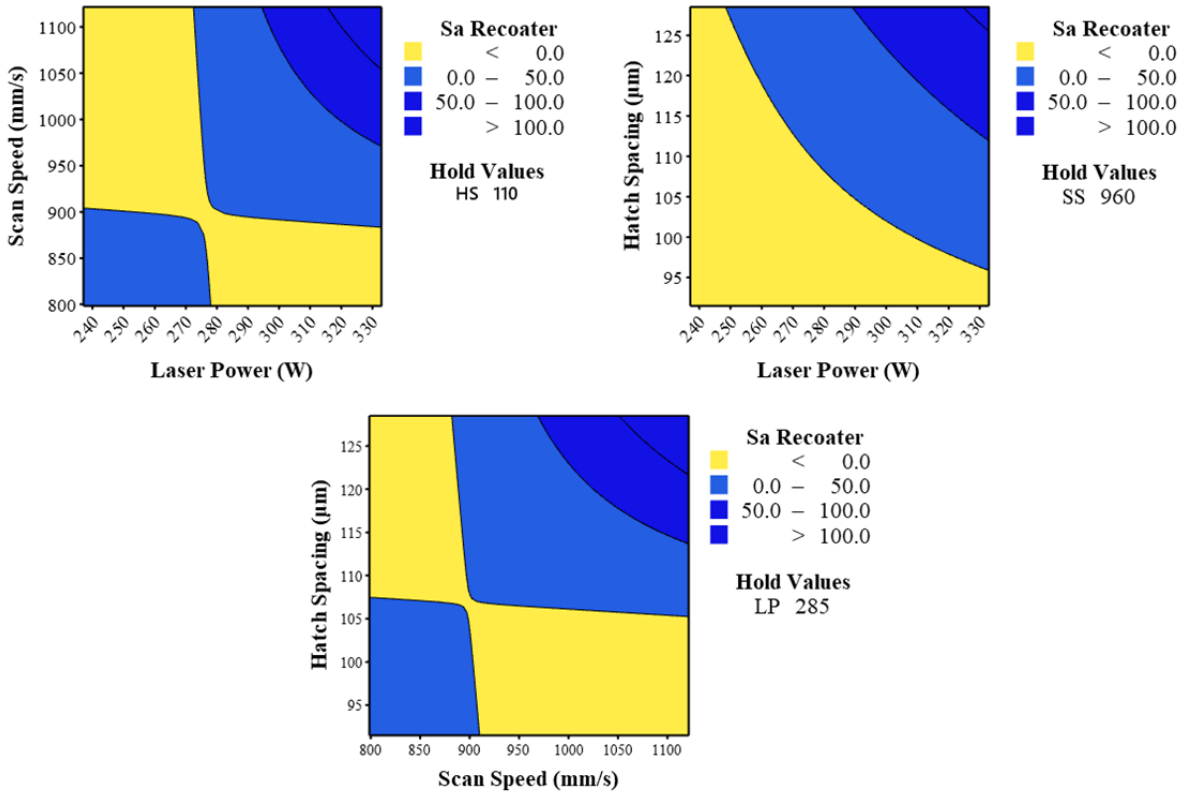

Figure 28: Contour plots showing the effect of different laser processing parameter on the surface roughness of different samples, the desired ranges for the surface roughness are presented in yellow areas. The regions in blue represent areas of surface which is higher than the desired value.

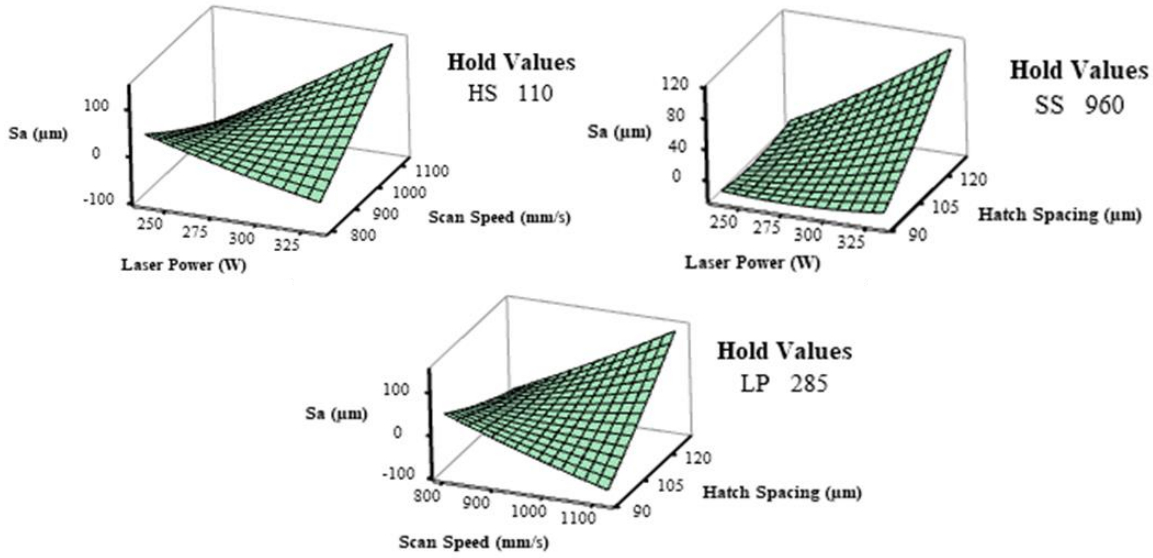

Figure 29: Surface plots showing the effect of different laser processing parameters on the surface roughness of different samples.

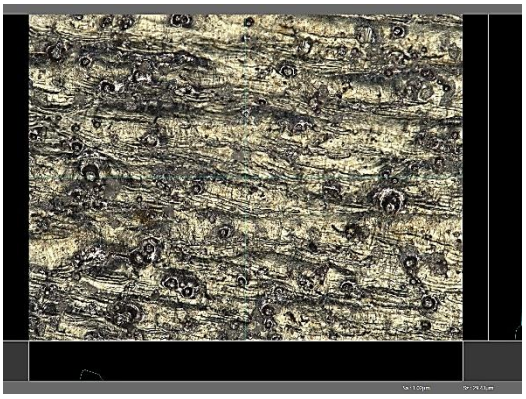

Figure 30: Surface roughness of sample fabricated with LP 285, SS 798.54 and HS 110 as measured using the Keyence VHX 7000 series microscope.

Roughness analysis were carried out on three sides (observer side- the side facing the observer, recoater side- the side facing the pool of fresh powder & argon side- the side facing the flow of argon) of the samples and the maximum height (Sz) and arithmetical mean height (Sa) were noted and are presented in Table 8. From the trend seen in the values for S_a and S_z for all samples and the regression analysis performed using Minitab, it is clear that surface roughness increases as the laser power increases.

Table 8: Average values of roughness on the sides facing the flow of Argon, facing the recoater, facing the observer of all samples

Laser Power (W)	Scan Speed (mm/s)	Hatch Spacing (µm)	Sa (Observer side)	Sz (Observer side)	Sa (Recoater side)	Sz (Recoater side)	Sa (Argon Side)	Sz (Argon Side)
256.5	864.0	99.0	9.417	65.677	6.980	46.763	6.967	49.710
256.5	864.0	121.0	4.933	43.580	5.030	41.030	5.193	47.540
313.5	864.0	121.0	5.253	52.143	3.983	33.067	4.677	53.143
237.1	960.0	110.0	7.170	58.540	6.045	33.795	5.090	48.697
285.0	960.0	110.0	5.483	55.873	7.690	52.693	5.643	51.830
313.5	864.0	99.0	6.550	52.770	6.443	45.280	6.610	54.883
256.5	1056.0	121.0	5.990	49.003	4.817	46.863	8.740	62.370
285.0	960.0	91.5	7.160	65.110	7.573	49.187	4.977	50.540
285.0	960.0	110.0	5.483	55.873	7.690	52.693	5.643	51.830
332.9	960.0	110.0	5.257	51.717	4.625	43.265	5.797	58.220
313.5	1056.0	121.0	6.543	50.943	180.890	42.527	4.680	41.853
285.0	798.5	110.0	4.987	41.793	2.905	30.760	6.860	68.553
285.0	960.0	110.0	4.927	53.350	4.973	46.197	6.757	48.187
285.0	1121.5	110.0	6.913	59.397	6.930	49.147	4.460	43.173
285.0	960.0	110.0	5.483	55.873	7.690	52.693	5.643	51.830
285.0	960.0	110.0	4.927	53.350	4.973	46.197	6.757	48.187
313.5	1056.0	99.0	6.303	56.257	5.027	36.570	4.810	53.880
285.0	960.0	128.5	7.773	50.813	6.410	47.967	4.860	50.480
256.5	1056.0	99.0	5.483	52.313	4.093	43.953	4.707	47.327
285.0	960.0	110.0	4.927	53.350	4.973	46.197	6.757	48.187

Chapter 5. Conclusions and Future Works

5.1. Conclusion

The motivation of this study primarily is to correlate the effect of process parameters on the properties of IN718 specimens using response surface methodology. Abiding to the principles of RSM methodologies and SLM process design, the following conclusions can be made with the help of the pareto charts:

- The interrelations among the various process parameters and geometrical dimensions like height, width and length were obtained. It was noted that the dimensions of the alloy specimen was affected by the scan speed. The deviation in height can be attributed to lack or abundance of thermal energy as numerous metallurgical characteristics like grain growth and epitaxial bonding are directly influenced by the variation in scan speed. Similarly, scan speed also impacts the width and length of the fabricated specimens.
- The compositional analysis using XRD revealed the presence of γ, γ', γ'' and δ phases in the as-built specimens. The scan speed influences the percentage of γ' in the fabricated IN718 parts. The scan speed plays a crucial role in defining the critical energy density levels which in turn defines the percentage (%) of γ and γ' phases.
- Hardness: this mechanical property was considered as it facilitates the correlation between the laser process parameters and the chemical composition. It is inferred that the scan speed square plays a significant role in determining the hardness of the fabricated IN718 parts. The scan speed and energy density are interdependent which thereby influences the temperature build up in the heat affected zones. As the compositional analysis revealed the presence of γ', γ'' strength hardening phases in the heat affected zones, the magnitude of hardness can be associated to the presence of the afore mentioned subsidiary phases.
- The roughness characteristics of an IN718 SLM built part can be influenced by a combination of mean, square and interaction of the laser process parameters. As the interaction between scan speed

and hatch spacing plays a significant role in determining the roughness of the fabricated IN718 parts, the value of roughness can directly be associated to the defects such as presence of unmelted powder and balling effect. The above-mentioned detrimental outcomes shall also influence the geometrical accuracy of the fabricated part.

5.2. Future Work

This study has investigated the idea of using design of experiments to correlate the effect of process parameters on the properties of SLM fabricated IN718. Some of the potential future trends are mentioned below:

- The effect of other process parameters such as laser beam diameter, different set of scan strategies like chess, stripe etc., layer thickness needs to be studied in order to correlate their effect on the properties of SLM fabricated IN718.
- The study can be further expanded to study the effect of laser process parameters on the microstructure by conducting SEM and EBSD analysis.
- δ phase being one of the most important phases of IN718 can be correlated with the effect of process parameters. This will help in controlling the percentage of δ phase in the fabricated samples.

References

[1] L. Zheng, G. Schmitz, Y. Meng, R. Chellali, R. Schlesiger, Mechanism of Intermediate Temperature Embrittlement of Ni and Ni-based Superalloys, Critical Reviews in Solid State and Materials Sciences (2012).

[2] D.F. Paulonis, J.J. Schirra, Alloy 718 at Pratt & Whitney–Historical perspective and future challenges, Superalloys (2001).

[3] S. Metals, Inconel alloy 718, Special Metals, 2007.

[4] L.C. Ardila, F. Garciandia, J.B. Gonzalez-Diaz, P. Alvarez, A. Echeverria, M. Petite, R. Deffley, J. Ochoa, Effect of IN718 Recycled Powder Reuse on Properties of Parts Manufactured by Means of Selective Laser Melting, Physics Procedia 56 (2014) 9.

[5] R.C. Reed, The Superalloys: Fundamentals and Applications, 2009.

[6] J.W. Brooks, P.J. Bridges, Metallurgical Stability of Inconel Alloy 718, Superalloys (1988).

[7] E.A. Loria, The Status and Prospects of Alloy 718, The Journal of The Minerals, Metals & Materials Society (1988) 6.

[8] D. Deng, Additively Manufactured Inconel 718 : Microstructures and Mechanical Properties, Departement of Management and Engineering, Linköping University, 2018.

[9] V.R. Rajendran, K. Mamidi, B. Ravichander, B. Farhang, A. Amerinatanzi, N.S. Moghaddam, Determination of residual stress for Inconel 718 samples fabricated through different scanning strategies in selective laser melting, Behavior and Mechanics of Multifunctional Materials IX, International Society for Optics and Photonics, 2020, p. 1137719.

[10] S. Srivathsan, B.B. Ravichander, N.S. Moghaddam, N. Swails, A. Amerinatanzi, Investigation of the strength of different porous lattice structures manufactured using selective laser melting, Behavior and Mechanics of Multifunctional Materials IX, International Society for Optics and Photonics, 2020, p. 113771B.

[11] M.J. Donachie, S.J. Donachie, Superalloys: a technical guide, ASM international (2002).

[12] R. Bowman, Superalloys: A Primer and History, 9th International Symposium on Superalloys, Champion, Pennsylvania, 2000.

[13] B. Seitz, METHODOLOGY FOR EFFICIENTLY ESTABLISHING PROCESSING-STRUCTURE-PROPERTY RELATIONSHIPS FOR ADDITIVE-MANUFACTURED AGE-HARDENED ALLOYS, George W. Woodruff School of Mechanical Engineering, Georgia Institute of Technology, 2016.

[14] H.K.D.H. Bhadeshia, Nickel Based Superalloys, (2016).

[15] J.M. Oblak, D.F. Paulonis, D.S. Duvall, Coherency strengthening in Ni base alloys hardened by DO_{22} γ' precipitates, Metallurgical Transactions (1974).

[16] S. Azadian, L.-Y. Wei, R. Warren, Delta phase precipitation in Inconel 718, Materials Characterization 53(1) (2004).

[17] J.K.Hong, J.H.Park, N.K.Park, I.S.Eom, M.B.Kim, C.Y.Kang, Microstructures and mechanical properties of Inconel 718 welds by CO_2 laser welding, Journal of Materials Processing Technology 201(1-3) (2008).

[18] G. Sjoberg, N.G. Ingesten, R.G. Carlson, Grain Boundary δ-Phase Morphologies, Carbides and Notch Rupture Sensitivity of Cast Alloy 718, Metals & Materials Society (1991).

[19] P. Scallan, Material evaluation and process selection, Process Planning (2003).

[20] R.G. Carlson, J.F. Radavich, MICROSTRUCTURAL CHARACTERIZATION OF CAST 718 International Symposium on Superalloys, 1989.

[21] G.A. Rao, M. Kumar, M. Srinivas, D.S. Sarma, Effect of standard heat treatment on the microstructure and mechanical properties of hot isostatically pressed superalloy Inconel 718, Materials Science and Engineering: A (2003).

[22] G.A. Rao, M. Srinivas, D.S. Sarma, Influence of modified processing on structure and properties of hot isostatically pressed superalloy Inconel 718, Materials Science and Engineering: A (2006).

[23] G.A. Rao, M. Srinivas, D.S. Sarma, Effect of oxygen content of powder on microstructure and mechanical properties of hot isostatically pressed superalloy Inconel 718, Materials Science and Engineering: A (2006).

[24] H. Dabbaghi, M. Nematollahi, K.S. Baghbaderani, P. Bayatimalayeri, M. Elahinia, High-Temperature Oxidation Kinetics of Additively Manufactured NiTiHf, arXiv preprint arXiv:2006.11114 (2020).

[25] J. Li, Z. Zhao, P. Bai, H. Qu, B. Liu, L. Li, L. Li, L. Wu, R. Guan, H. Liu, Z. Guo, Microstructural evolution and mechanical properties of IN718 alloy fabricated by selective laser melting following different heat treatments, Journal of Alloys and Compunds 772 (2019) 10.

[26] M. Pouranvari, A. Ekrami, A.H. Kokabi, Transient liquid phase bonding of wrought IN718 nickel based superalloy using standard heat treatment cycles: Microstructure and mechanical properties, Materials & Design 50 (2013).

[27] D. Zhang, Z. Feng, C. Wang, W. Wang, Z. Liu, W. Niu, Comparison of microstructures and mechanical properties of Inconel 718 alloy processed by selective laser melting and casting, Materials Science and Engineering: A 724 (2018).

[28] M. Elahinia, N.S. Moghaddam, M.T. Andani, A. Amerinatanzi, B.A. Bimber, R.F. Hamilton, Fabrication of NiTi through additive manufacturing: A review, Progress in Materials Science 83 (2016) 630-663.

[29] A. Jahadakbar, M. Nematollahi, K. Safaei, P. Bayati, G. Giri, H. Dabbaghi, D. Dean, M. Elahinia, Design, Modeling, Additive Manufacturing, and Polishing of Stiffness-Modulated Porous Nitinol Bone Fixation Plates Followed by Thermomechanical and Composition Analysis, Metals 10(1) (2020) 151.

[30] N.S. Moghaddam, S.E. Saghaian, A. Amerinatanzi, H. Ibrahim, P. Li, G.P. Toker, H.E. Karaca, M. Elahinia, Anisotropic tensile and actuation properties of NiTi fabricated with selective laser melting, Materials Science and Engineering: A 724 (2018) 220-230.

[31] B. Farhang, B.B. Ravichander, F. Venturi, A. Amerinatanzi, N.S. Moghaddam, Study on variations of microstructure and metallurgical properties in various heat-affected zones of SLM fabricated Nickel–Titanium alloy, Materials Science and Engineering: A (2020) 138919.

[32] N.S. Moghaddam, A. Jahadakbar, A. Amerinatanzi, M. Elahinia, Recent advances in laser-based additive manufacturing, Laser-Based Additive Manufacturing of Metal Parts, CRC Press2017, pp. 1-24.

[33] G.G. Berdine, M. DiPaola, M. Weinberg, Economic and Regulatory Perspectives on Additive Manufacturing, 3D Printing in Orthopaedic Surgery, Elsevier2019, pp. 41-48.

[34] M.T. Andani, N.S. Moghaddam, C. Haberland, D. Dean, M.J. Miller, M. Elahinia, Metals for bone implants. Part 1. Powder metallurgy and implant rendering, Acta biomaterialia 10(10) (2014) 4058-4070.

[35] B. Baufeld, E. Brandl, O. Van der Biest, Wire based additive layer manufacturing: Comparison of microstructure and mechanical properties of Ti–6Al–4V components fabricated by laser-beam deposition and shaped metal deposition, Journal of Materials Processing Technology 211(6) (2011) 1146-1158.

[36] H. Dabbaghi, K. Safaei, M. Nematollahi, P. Bayati, M. Elahinia, Additively Manufactured NiTi and NiTiHf Alloys: Estimating Service Life in High-Temperature Oxidation, Materials 13(9) (2020) 2104.

[37] I. Gibson, D. Rosen, B. Stucker, Additive Manufacturing Technologies, 2 ed.2015.

[38] EOS-GmbH, History, 2014. http://www.eos.info/about_eos/history.

[39] M. Attaran, The rise of 3-D printing: The advantages of additive manufacturing over traditional manufacturing, Business Horizons 60(5) (2017).

[40] C. Deckard, J. Beaman, Selective Laser Sintering, Birth of an Industry, 2012.

[41] C.R. Deckard, Method and apparatus for producing parts by selective sintering, USA, 1986.

[42] L.-E. Andersson, M. Larsson, DEVICE AND ARRANGEMENT FOR PRODUCING A THREE-DIMENSIONAL OBJECT Arcam AB, USA, 2001.

[43] J.M. Pearce, C.M. Blair, K.J. Laciak, R. Andrews, A. Nosrat, I. Zelenika-Zovko, 3-D Printing of Open Source Appropriate Technologies for Self-Directed Sustainable Development Journal of Sustainable Development 3 (2010).

[44] B. Berman, 3-D printing: The new industrial revolution, Business Horizons 55 (2012).

[45] J.-P. Kruth, G. Levy, F. Klocke, T.H.C. Childs, Consolidation phenomena in laser and powder-bed based layered manufacturing, CIRP Annals 56(2) (2007).

[46] R.I. Campbell, D. Bourell, I. Gibson, Additive manufacturing: Rapid prototyping comes of age, Rapid Prototyping Journal (2012).

[47] D. Hu, H. Mei, R. Kovacevic, Improving solid freeform fabrication by laser-based additive manufacturing, Proceedings of the Institution of Mechanical Engineers, Part B: Journal of Engineering Manufacture, 2002.

[48] B. Baufeld, E. Brandl, O.V.d. Biest, Wire based additive layer manufacturing: Comparison of microstructure and mechanical properties of Ti–6Al–4V components fabricated by laser-beam deposition and shaped metal deposition, Journal of Materials Processing Technology (2011).

[49] A. MT, S.M. N, H. C, D. D, M. MJ, E. M, Metals for bone implants. Part 1. Powder metallurgy and implant rendering, Acta Biomater (2014).

[50] P.J. Andersen, S.K. Hodson, Articles of manufacture and methods for manufacturing laminate structures including inorganically filled sheets, USA, 1998.

[51] B. Xiao, Y. Zhang, Laser sintering of metal powders on top of sintered layers under multiple-line laser scanning, Journal of Physics D: Applied Physics 40 (2007).

[52] D. Ding, Z. Pan, D. Cuiuri, H. Li, A multi-bead overlapping model for robotic wire and arc additive manufacturing (WAAM), Robotics and Computer-Integrated Manufacturing 31 (2015).

[53] M.H. Elahinia, Shape Memory Alloy Actuators: Design, Fabrication and Experimental Evaluation, John Wiley & Sons2015.

[54] I.V. Shishkovsky, L.T. Volova, M.V. Kuznetsov, Y.G. Morozov, I.P. Parkin, Porous biocompatible implants and tissue scaffolds synthesized by selective laser sintering from Ti and NiTi. Journal of Materials Chemistry, Journal of Materials Chemistry (12) (2008).

[55] M.H. Elahinia, M. Hashemi, M. Tabesh, S.B. Bhaduri, Manufacturing and processing of NiTi implants: A review, Progress in Materials Science 57(5) (2012).

[56] S.C. Danforth, M. Agarwala, A. Bandyopadghyay, N. Langrana, V.R. Jamalabad, A. Safari, R.V. Weeren, Solid freeform fabrication methods, USA, 1998.

[57] A. Bandyopadhyay, T.P. Gualtieri, S. Bose, Global Engineering and Additive Manufacturing, Additive Manufacturing (2015) 1.

[58] M. Khaing, J. Fuh, L. Lu, Direct metal laser sintering for rapid tooling: processing and characterisation of EOS parts, Journal of Materials Processing Technology 113(1) (2001) 269-272.

[59] S. Kolossov, E. Boillat, R. Glardon, P. Fischer, M. Locher, 3D FE simulation for temperature evolution in the selective laser sintering process, International Journal of Machine Tools and Manufacture 44(2) (2004) 117-123.

[60] M. Agarwala, D. Bourell, J. Beaman, H. Marcus, J. Barlow, Direct selective laser sintering of metals, Rapid Prototyping Journal 1(1) (1995) 26-36.

[61] J.-P. Kruth, X. Wang, T. Laoui, L. Froyen, Lasers and materials in selective laser sintering, Assembly Automation 23(4) (2003) 357-371.

[62] J. Goban, M. Semancík, T. Lazoríková, Manufacturing of forms for injection moulding technology by rapid prototyping method, Annals of the Faculty of Engineering Hunedoara 11(1) (2013) 195.

[63] M. Shellabear, O. Nyrhilä, DMLS-Development history and state of the art, Laser Assisted Netshape Engineering 4, Proceedings of the 4th LANE (2004) 21-24.

[64] I. Gibson, D.W. Rosen, B. Stucker, Additive manufacturing technologies, Springer2010.

[65] D. Gu, Y.-C. Hagedorn, W. Meiners, G. Meng, R.J.S. Batista, K. Wissenbach, R. Poprawe, Densification behavior, microstructure evolution, and wear performance of selective laser melting processed commercially pure titanium, Acta Materialia 60(9) (2012) 3849-3860.

[66] I. Yadroitsev, I. Smurov, Selective laser melting technology: from the single laser melted track stability to 3D parts of complex shape, Physics Procedia 5 (2010) 551-560.

[67] S. Huang, F. You, H. Peng, W. Luo, Y. Feng, S. Lv, L. Sun, C. Yan, Influence of surface on spectroscopic properties of rare earth ions in nanocrystals, Journal of Rare Earth 25(4) (2007) 396-401.

[68] M. Elahinia, N.S. Moghaddam, M.T. Andani, R. Rahmanian, J. Walker, M. Miller, D. Dean, Site-specific material properties and the additive manufacturing of nitinol musculoskeletal implants, Tissue Engineering Part A, MARY ANN LIEBERT, INC 140 HUGUENOT STREET, 3RD FL, NEW ROCHELLE, NY 10801 USA, 2014, pp. S120-S121.

[69] A. Amerinatanzi, H. Zamanian, N. Shayesteh Moghaddam, A. Jahadakbar, M. Elahinia, Application of the superelastic NiTi spring in ankle foot orthosis (AFO) to create normal ankle joint behavior, Bioengineering 4(4) (2017) 95.

[70] N. Moghaddam, A. Amerinatanzi, S. Saedi, A. Turabi, H. Karaca, M. Elahinia, Stiffness Tuning of Niti Implants Through Aging, V001T02A014-V001T02A014 (2016).

[71] K.A. Mumtaz, P. Erasenthiran, N. Hopkinson, High density selective laser melting of Waspaloy®, Journal of materials processing technology 195(1) (2008) 77-87.

[72] B. Zhang, H. Liao, C. Coddet, Microstructure evolution and density behavior of CP Ti parts elaborated by self-developed vacuum selective laser melting system, Applied surface science 279 (2013) 310-316.

[73] L. Dong, H. Wang, Microstructure and corrosion properties of laser-melted deposited Ti2Ni3Si/NiTi intermetallic alloy, Journal of Alloys and Compounds 465(1-2) (2008) 83-89.

[74] B. Zhang, H. Liao, C. Coddet, Selective laser melting commercially pure Ti under vacuum, Vacuum 95 (2013) 25-29.

[75] S. Saedi, S.E. Saghaian, A. Jahadakbar, N.S. Moghaddam, M.T. Andani, S.M. Saghaian, Y.C. Lu, M. Elahinia, H.E. Karaca, Shape memory response of porous NiTi shape memory alloys fabricated by selective laser melting, Journal of Materials Science: Materials in Medicine 29(4) (2018) 40.

[76] A. Ahmadi, N. Shayesteh Moghaddam, M. Elahinia, H.E. Karaca, R. Mirzaeifar, Finite element modeling of selective laser melting 316l stainless steel parts for evaluating the mechanical properties, International Manufacturing Science and Engineering Conference, American Society of Mechanical Engineers, 2016, p. V002T01A003.

[77] N.S. Moghaddam, A. Jahadakbar, M. Elahinia, D. Dean, M. Miller, The effect of adding dental implants to the reconstructed mandible comparing the effect of using Ti-6Al-4V and NiTi hardware, Tissue Engineering Part A, MARY ANN LIEBERT, INC 140 HUGUENOT STREET, 3RD FL, NEW ROCHELLE, NY 10801 USA, 2015, pp. S398-S398.

[78] S. Thakare, B.B. Ravichander, N. Swails, N.S. Moghaddam, A. Amerinatanzi, The effect of support structure geometry on surface topography of selectively laser melted parts, Behavior and Mechanics of Multifunctional Materials IX, International Society for Optics and Photonics, 2020, p. 113771D.

[79] A. Jahadakbar, N.S. Moghaddam, A. Amerinatanzi, D. Dean, M. Elahinia, Mechanical evaluation of the SLM fabricated, stiffness-matched, mandibular bone fixation plates, Behavior and Mechanics of Multifunctional Materials and Composites XII, International Society for Optics and Photonics, 2018, p. 1059610.

[80] N.S. Moghaddam, S. Saedi, A. Amerinatanzi, E. Saghaian, A. Jahadakbar, H. Karaca, M. Elahinia, Selective laser melting of Ni-rich NiTi: selection of process parameters and the superelastic response, Behavior and Mechanics of Multifunctional Materials and Composites XII, International Society for Optics and Photonics, 2018, p. 105960W.

[81] M.J. Ashrafi, A. Amerinatanzi, Z. Saebi, N.S. Moghaddam, R. Mehrabi, H. Karaca, M. Elahinia, Shape memory response of cellular lattice structures: Unit cell finite element prediction, Mechanics of Materials 125 (2018) 26-34.

[82] P. Mercelis, J.-P. Kruth, Residual stresses in selective laser sintering and selective laser melting, Rapid Prototyping Journal 12(5) (2006) 254-265.

[83] R. Knight, J. Wright, J. Beaman, D. Freitag, Metal processing using selective laser sintering and hot isostatic pressing (SLS/HIP), Proceedings of the Solid Freeform Fabrication Symposium, 1996, pp. 349-353.

[84] S. Das, M. Wohlert, J.J. Beaman, D.L. Bourell, Processing of titanium net shapes by SLS/HIP, Materials & design 20(2) (1999) 115-121.

[85] P. Regenfuss, R. Ebert, H. Exner, Laser micro sintering–a versatile Instrument for the generation of microparts, Laser Technik Journal 4(1) (2007) 26-31.

[86] P. Regenfuss, L. Hartwig, S. Klotzer, R. Ebert, H. Exner, Microparts by a novel modification of selective laser sintering, TECHNICAL PAPERS-SOCIETY OF MANUFACTURING ENGINEERS-ALL SERIES- (2004).

[87] P. Regenfuss, L. Hartwig, S. Klötzer, R. Ebert, T. Brabant, T. Petsch, H. Exner, Industrial freeform generation of microtools by laser micro sintering, Rapid Prototyping Journal 11(1) (2005) 18-25.

[88] M. Aliakbari, Additive manufacturing: State-of-the-art, capabilities, and sample applications with cost analysis, (2012).

[89] R. Udroiu, POWDER BED ADDITIVE MANUFACTURING SYSTEMS AND ITS APPLICATIONS, Academic journal of manufacturing engineering 10(4) (2012).

[90] V. Petrovic, J. Vicente Haro Gonzalez, O. Jordá Ferrando, J. Delgado Gordillo, J. Ramón Blasco Puchades, L. Portolés Griñan, Additive layered manufacturing: sectors of industrial application shown through case studies, International Journal of Production Research 49(4) (2011) 1061-1079.

[91] S. Saedi, A.S. Turabi, M.T. Andani, N.S. Moghaddam, M. Elahinia, H.E. Karaca, Texture, aging, and superelasticity of selective laser melting fabricated Ni-rich NiTi alloys, Materials Science and Engineering: A 686 (2017) 1-10.

[92] R. Rahmanian, N.S. Moghaddam, C. Haberland, D. Dean, M. Miller, M. Elahinia, Load bearing and stiffness tailored niti implants produced by additive manufacturing: a simulation study, Behavior and Mechanics of Multifunctional Materials and Composites 2014, International Society for Optics and Photonics, 2014, p. 905814.

[93] A. Jahadakbar, N. Shayesteh Moghaddam, A. Amerinatanzi, D. Dean, H.E. Karaca, M. Elahinia, Finite element simulation and additive manufacturing of stiffness-matched niti fixation hardware for mandibular reconstruction surgery, Bioengineering 3(4) (2016) 36.

[94] A. Dehghanghadikolaei, H. Ibrahim, A. Amerinatanzi, M. Hashemi, N.S. Moghaddam, M. Elahinia, Improving corrosion resistance of additively manufactured nickel–titanium biomedical devices by micro-arc oxidation process, Journal of materials science 54(9) (2019) 7333-7355.

[95] N.S. Moghaddam, M. Elahinia, M. Miller, D. Dean, Enhancement of bone implants by substituting nitinol for titanium (Ti-6Al-4V): A modeling comparison, Smart Materials, Adaptive Structures and Intelligent Systems, American Society of Mechanical Engineers, 2014, p. V001T03A031.

[96] H.D. Dean, M.H. Elahinia, C. Haberland, M.J. Miller, A. Sutradhar, N.S. Moghaddam, J.M. Walker, R. Skoracki, Methods, devices, and manufacture of the devices for musculoskeletal reconstructive surgery, Google Patents, 2017.

[97] A. Hadi, M. Qasemi, M. Elahinia, N. Moghaddam, Modeling and experiment of a flexible module actuated by shape memory alloy wire, Smart Materials, Adaptive Structures and Intelligent Systems, American Society of Mechanical Engineers, 2014, p. V001T03A035.

[98] B. Raad, N.S. Moghaddam, M. Elahinia, A numerical simulation of the effect of using porous superelastic Nitinol and stiff Titanium fixation hardware on the bone remodeling, Nanosensors, Biosensors, and Info-Tech Sensors and Systems 2016, International Society for Optics and Photonics, 2016, p. 98021T.

[99] N.S. Moghaddam, A. Jahadakbar, A. Amerinatanzi, M. Elahinia, Recent Advances in Laser Based Additive Manufacturing Laser-Based Additive Manufacturing of Metal Parts, Taylor & Francis Group2017.

[100] E.C. Santos, M. Shiomi, K. Osakada, T. Laoui, Rapid manufacturing of metal components by laser forming, International Journal of Machine Tools and Manufacture 46(12) (2006) 1459-1468.

[101] S. Kumar, Selective laser sintering: a qualitative and objective approach, Jom 55(10) (2003) 43-47.

[102] H. Zhu, L. Lu, J. Fuh, Development and characterisation of direct laser sintering Cu-based metal powder, Journal of Materials Processing Technology 140(1) (2003) 314-317.

[103] P. Fischer, V. Romano, A. Blatter, H. Weber, Highly precise pulsed selective laser sintering of metallic powders, Laser Physics Letters 2(1) (2005) 48-55.

[104] H. Schleifenbaum, W. Meiners, K. Wissenbach, C. Hinke, Individualized production by means of high power Selective Laser Melting, CIRP Journal of manufacturing science and technology 2(3) (2010) 161-169.

[105] T. Kaiser, G.J. Albrecht, Industrial Disk Lasers for Micro Material Processing–Compact Reliable Systems Conquer the Market, Laser Technik Journal 4(3) (2007) 54-57.

[106] S. Das, M. Wohlert, J. Beaman, D. Bourell, Direct selective laser sintering and containerless hot isostatic pressing for high performance metal components, Proceedings to the Solid Freeform Fabrication Symposium, 1997.

[107] B. Xiao, Y. Zhang, Laser sintering of metal powders on top of sintered layers under multiple-line laser scanning, Journal of Physics D: Applied Physics 40(21) (2007) 6725.

[108] J. Hänninen, DMLS moves from rapid tooling to rapid manufacturing, Metal Powder Report 56(9) (2001) 24-29.

[109] M.K. Ravari, M. Kadkhodaei, A. Ghaei, A microplane constitutive model for shape memory alloys considering tension–compression asymmetry, Smart Materials and Structures 24(7) (2015) 075016.

[110] J.-P. Kruth, L. Froyen, J. Van Vaerenbergh, P. Mercelis, M. Rombouts, B. Lauwers, Selective laser melting of iron-based powder, Journal of Materials Processing Technology 149(1) (2004) 616-622.

[111] F. Abe, K. Osakada, M. Shiomi, K. Uematsu, M. Matsumoto, The manufacturing of hard tools from metallic powders by selective laser melting, Journal of materials processing technology 111(1) (2001) 210-213.

[112] T. Childs, C. Hauser, M. Badrossamay, Selective laser sintering (melting) of stainless and tool steel powders: experiments and modelling, Proceedings of the Institution of Mechanical Engineers, Part B: Journal of Engineering Manufacture 219(4) (2005) 339-357.

[113] J. Delgado, J. Ciurana, C.A. Rodríguez, Influence of process parameters on part quality and mechanical properties for DMLS and SLM with iron-based materials, The International Journal of Advanced Manufacturing Technology 60(5-8) (2012) 601-610.

[114] Z. Wang, K. Guan, M. Gao, X. Li, X. Chen, X. Zeng, The microstructure and mechanical properties of deposited-IN718 by selective laser melting, Journal of Alloys and Compunds 513 (2012) 6.

[115] N.S. Moghaddam, S. Saedi, A. Amerinatanzi, A. Hinojos, A. Ramazani, J. Kundin, M.J. Mills, H. Karaca, M. Elahinia, Achieving superelasticity in additively manufactured NiTi in compression without post-process heat treatment, (2019).

[116] K.N. Amato, S.M. Gaytan, L.E. Murr, E. Martinez, P.W. Shindo, J. Hernandez, S. Collins, F. Medina, Microstructures and mechanical behavior of Inconel 718 fabricated by selective laser melting, Acta Materialia 60(5) (2012).

[117] Q. Jia, D. Gu, Selective laser melting additive manufacturing of Inconel 718 superalloy parts: Densification, microstructure and properties, Journal of Alloys and Compunds 585 (2014).

[118] D. Zhang, W. Niu, X. Cao, Z. Liu, Effect of standard heat treatment on the microstructure and mechanical properties of selective laser melting manufactured Inconel 718 superalloy, Materials Science and Engineering: A 644 (2015).

[119] E. Chlebus, K. Gruber, B. Kuźnicka, J.Kurzac, T.Kurzynowski, Effect of heat treatment on the microstructure and mechanical properties of Inconel 718 processed by selective laser melting, Materials Science and Engineering: A 639 (2015).

[120] F. Brenne, A. Taube, M. Pröbstle, S. Neumeier, D. Schwarze, M. Schaper, T. Niendorf, Microstructural design of Ni-base alloys for high-temperature applications: impact of heat treatment on microstructure and mechanical properties after selective laser melting, Progress in Additive Manufacturing (2016).

[121] W.M. Tucho, P. Cuvillier, A. Sjolyst-Kverneland, V. Hansen, Microstructure and hardness studies of Inconel 718 manufactured by selective laser melting before and after solution heat treatment, Materials Science and Engineering: A 689 (2017).

[122] M. Pröbstle, S. Neumeier, J. Hopfenmüller, L. Freund, T. Niendorf, D. Schwarze, M. Göken, Superior creep strength of a nickel-based superalloy produced by selective laser melting, Materials Science and Engineering: A (2016).

[123] O. Es-Said, J. Foyos, R. Noorani, M. Mendelson, R. Marloth, B. Pregger, Effect of layer orientation on mechanical properties of rapid prototyped samples, Materials and Manufacturing Processes 15(1) (2000) 107-122.

[124] M. Elahinia, N.S. Moghaddam, A. Amerinatanzi, S. Saedi, G.P. Toker, H. Karaca, G.S. Bigelow, O. Benafan, Additive manufacturing of NiTiHf high temperature shape memory alloy, Scripta Materialia 145 (2018) 90-94.

[125] A. Ahmadi, R. Mirzaeifar, N.S. Moghaddam, A.S. Turabi, H.E. Karaca, M. Elahinia, Effect of manufacturing parameters on mechanical properties of 316L stainless steel parts fabricated by selective laser melting: A computational framework, Materials & Design 112 (2016) 328-338.

[126] C. Ma, M.T. Andani, H. Qin, N.S. Moghaddam, H. Ibrahim, A. Jahadakbar, A. Amerinatanzi, Z. Ren, H. Zhang, G.L. Doll, Improving surface finish and wear resistance of additive manufactured nickel-titanium by ultrasonic nano-crystal surface modification, Journal of Materials Processing Technology 249 (2017) 433-440.

[127] H. Ibrahim, A. Jahadakbar, A. Dehghan, N.S. Moghaddam, A. Amerinatanzi, M. Elahinia, In vitro corrosion assessment of additively manufactured porous NiTi structures for bone fixation applications, Metals 8(3) (2018) 164.

[128] S.N. Esfahani, M.T. Andani, N.S. Moghaddam, R. Mirzaeifar, M. Elahinia, Independent tuning of stiffness and toughness of additively manufactured titanium-polymer composites: Simulation, fabrication, and experimental studies, Journal of Materials Processing Technology 238 (2016) 22-29.

[129] N.S. Moghaddam, A. Jahadakbar, A. Amerinatanzi, M. Elahinia, M. Miller, D. Dean, Metallic fixation of mandibular segmental defects: Graft immobilization and orofacial functional maintenance, Plastic and Reconstructive Surgery Global Open 4(9) (2016).

[130] N.S. Moghaddam, M.T. Andani, A. Amerinatanzi, C. Haberland, S. Huff, M. Miller, M. Elahinia, D. Dean, Metals for bone implants: Safety, design, and efficacy, Biomanufacturing Reviews 1(1) (2016) 1.

[131] S. Saedi, N.S. Moghaddam, A. Amerinatanzi, M. Elahinia, H.E. Karaca, On the effects of selective laser melting process parameters on microstructure and thermomechanical response of Ni-rich NiTi, Acta Materialia 144 (2018) 552-560.

[132] N.S. Moghaddam, R. Skoracki, M. Miller, M. Elahinia, D. Dean, Three dimensional printing of stiffness-tuned, nitinol skeletal fixation hardware with an example of mandibular segmental defect repair, Procedia CIRP 49 (2016) 45-50.

[133] N. Shayesteh Moghaddam, Toward patient specific long lasting metallic implants for mandibular segmental defects, University of Toledo, 2015.

[134] M.E. Aydinöz, F. Brenne, M. Schaper, C. Schaak, W. Tillmann, J. Nellesen, T. Niendorf, On the microstructural and mechanical properties of post-treated additively manufactured Inconel 718 superalloy under quasistatic and cyclic loading, Materials Science and Engineering: A (2016).

[135] K. Mamidi, H.K. Talla, B.B. Ravichander, B. Farhang, N.S. Moghaddam, A. Amerinatanzi, Study on the influence of post-processing parameters over microstructure and metallurgical properties of NiTi alloy, Behavior and Mechanics of Multifunctional Materials IX, International Society for Optics and Photonics, 2020, p. 113770V.

[136] J.H. Yi, J.W. Kang, T.J. Wang, X. Wang, Y.Y. Hu, T. Feng, Y.L. Feng, P.Y. Wu, Effect of laser energy density on the microstructure, mechanical properties, and deformation of Inconel 718 samples fabricated by selective laser melting, Journal of Alloys and Compounds 786 (2019).

[137] M. Sadowski, L. Ladani, W. Brindley, J. Romano, Optimizing quality of additively manufactured Inconel 718 using powder bed laser melting process, Additive Manufacturing 11 (2016).

[138] Q. Shi, D. Gu, M. Xia, S. Cao, T. Rong, Effects of laser processing parameters on thermal behavior and melting/solidification mechanism during selective laser melting of TiC/Inconel 718 composites, Optics and Lasers Technology 84 (2016).

[139] D. Buchbinder, W. Meiners, N. Pirch, K. Wissenbach, J. Schrage, Investigation on reducing distortion by preheating during manufacture of aluminum components using selective laser melting, Journal of Laser Applications (2014).

[140] X. Han, H. Zhu, X. Nie, G. Wang, X. Zeng, Investigation on Selective Laser Melting AlSi10Mg Cellular Lattice Strut: Molten Pool Morphology, Surface Roughness and Dimensional Accuracy, Materials (2018).

[141] D. Wang, S. Wu, Y. Bai, H. Lin, Y. Yang, C. Song, Characteristics of typical geometrical features shaped by selective laser melting, Journal of Laser Applications (2017).

[142] B.B. Ravichander, B. Farhang, N. Swails, A. Amerinatanzi, N.S. Moghaddam, Analysis of the deviation in properties of selective laser melted samples fabricated by varying process parameters, Behavior and Mechanics of Multifunctional Materials IX, International Society for Optics and Photonics, 2020, p. 113771A.

[143] X. Gong, X. Wang, Z. Jones, K. Cooper, J.V. Cole, K. Chou, Characterization of Microstructure and Mechanical Property of Inconel 718 from Selective Laser Melting, ASME 2015 International Manufacturing Science and Engineering Conference, Charlotte, North Carolina, 2015.

[144] W. Tillmann, C. Schaak, J. Nellesen, M. Schaper, M.E. Aydinöz, K.-P. Hoyer, Hot isostatic pressing of IN718 components manufactured by selective laser melting, Additive Manufacturing (2016) 10.

[145] G. E.Bean, D. B.Witkin, T. D.McLouth, D. N.Patel, R. J.Zaldivar, Effect of laser focus shift on surface quality and density of Inconel 718 parts produced via selective laser melting, Additive Manufacturing 22 (2018).

[146] C. Yan, L. Hao, A. Hussein, P. Young, D. Raymont, Advanced lightweight 316L stainless steel cellular lattice structures fabricated via selective laser melting, Materials & Design 55 (2014).

[147] K. Mumtaz, N. Hopkinson, Top surface and side roughness of Inconel 625 parts processed using selective laser melting, Rapid Prototyping Journal (2009).

[148] K. Alrbaey, D. Wimpenny, R. Tosi, W. Manning, A. Moroz, On Optimization of Surface Roughness of Selective Laser Melted Stainless Steel Parts: A Statistical Study, Journal of Materials Engineering and Performance (2014).

[149] J.-P. Choi, G.-H. Shin, S. Yang, D.-Y. Yang, J.-S. Lee, M. Brochu, J.-H. Yu, Densification and microstructural investigation of Inconel 718 parts fabricated by selective laser melting, Powder Technology (2017).

[150] J. Strößner, M. Terock, U. Glatzel, Mechanical and Microstructural Investigation of Nickel-Based Superalloy IN718 Manufactured by Selective Laser Melting (SLM), Advanced Engineering Materials (2015).

[151] A.A. Popovich, V.S. Sufiiarov, I.A. Polozov, E.V. Borisov, Microstructure and mechanical properties of Inconel 718 produced by SLM and subsequent heat treatment, Key Engineering Materials (2015).

[152] D.H. Smith, J. Bicknell, L. Jorgensen, B.M. Patterson, N.L. Cordes, I. Tsukrov, M. Knezevic, Microstructure and mechanical behavior of direct metal laser sintered Inconel alloy 718, Materials Characterization (2016).

[153] Y.-L. Kuo, S. Horikawa, K. Kakehi, The effect of interdendritic δ phase on the mechanical properties of Alloy 718 built up by additive manufacturing Materials & Design (2016).

[154] X. Wang, K. Chou, Electron Backscatter Diffraction Analysis of Inconel 718 Parts Fabricated by Selective Laser Melting Additive Manufacturing, Journal of Materials (2016).

[155] A. Huxol, F.-J. Villmer, DoE Methods for Parameter Evaluation in Selective Laser Melting, IFAC-PapersOnLine 52(10) (2019).

[156] J. Antony, Design of Experiments for Engineers and Scientists, Elsevier2014.

[157] J.P.C. Kleijnen, Design Of Experiments: Overview, Winter Simulation Conference, 2008.

[158] NorikoRead, W. Wang, K. Essa, M.M. attallah, Selective laser melting of AlSi10Mg alloy: Process optimisation and mechanical properties development, Materials & Design 65 (2015) 8.

[159] A.H. Maamoun, Y.F. Xue, M.A. Elbestawi, S.C. Veldhuis, Effect of Selective Laser Melting Process Parameters on the Quality of Al Alloy Parts: Powder Characterization, Density, Surface Roughness, and Dimensional Accuracy, Materials (2018) 23.

[160] J.-R. Zhuang, Y.-T. Lee, W.-H. Hsieh, A.-S. Yang, Determination of melt pool dimensions using DOE-FEM and RSM with process window during SLM of Ti6Al4V powder, Optics and Lasers Technology 103 (2018).

[161] JianfengSun, YongqiangYang, DiWang, Parametric optimization of selective laser melting for forming Ti6Al4V samples by Taguchi method, Optics and Lasers Technology 49 (2013).

[162] A. Khorasani, I. Gibson, U.S. Awan, A. Ghaderi, The effect of SLM process parameters on density, hardness, tensile strength and surface quality of Ti-6Al-4V, Additive Manufacturing 25 (2019).

[163] N.S. Moghaddam, A. Jahadakbar, A. Amerinatanzi, R. Skoracki, M. Miller, D. Dean, M. Elahinia, Fixation Release and the Bone Bandaid: A New Bone Fixation Device Paradigm, Bioengineering (2017).

[164] A. Amerinatanzi, R. Summers, K. Ahmadi, V.K. Goel, T.E. Hewett, E. Nyman Jr, A novel 3d approach for determination of frontal and coronal plane tibial slopes from mr imaging, The Knee 24(2) (2017) 207-216.

[165] M. AH, X. YF, E. MA, V. SC, Effect of Selective Laser Melting Process Parameters on the Quality of Al Alloy Parts: Powder Characterization, Density, Surface Roughness, and Dimensional Accuracy., Materials (2018).